

ESCUELA POLITÉCNICA SUPERIOR DE MONDRAGON
UNIBERTSITATEA
MONDRAGON UNIBERTSITATEKO GOI ESKOLA POLITEKNIKOA
MONDRAGON UNIVERSITY FACULTY OF ENGINEERING

Trabajo presentado para la obtención del título de

Titulua eskuratzeko lana

Final degree project for taking the degree of

GRADO EN INGENIERÍA MECÁNICA
MEKANIKAKO INGENIARITZA GRADUA
DEGREE IN MECHANICAL ENGINEERING

Título del Trabajo *Lanaren izenburua* Project Topic

**3D SYNTHETIC MICROSTRUCTURE GENERATION INVOLVING
GRAIN SIZE, SHAPE, AND ORIENTATION REPRESENTATION**

Autor *Egilea* Author

SHEILA LIZARDI SCHAD

Curso *Ikasturtea* Year

2020/2021

Título del Trabajo *Lanaren izenburua* Project Topic

**3D SYNTHETIC MICROSTRUCTURE GENERATION
INVOLVING GRAIN SIZE, SHAPE, AND ORIENTATION
REPRESENTATION**

Nombre y apellidos del autor

Egilearen izen-abizenak

Author's name and surnames

LIZARDI SCHAD, SHEILA

Nombre y apellidos del/los director/es del trabajo

Zuzendariaren/zuzendarien izen-abizenak

Project director's name and surnames

JUNHE LIAN

MENDIGUREN, JOSEBA

Lugar donde se realiza el trabajo

Lana egin deneko lekua

Company where the project is being developed

Aalto University

Curso académico

Ikasturtea

Academic year

2020/2021



El autor/la autora del Trabajo Fin de Grado, autoriza a la Escuela Politécnica Superior de Mondragon Unibertsitatea, con carácter gratuito y con fines exclusivamente de investigación y docencia, los derechos de reproducción y comunicación pública de este documento siempre que: se cite el autor/la autora original, el uso que se haga de la obra no sea comercial y no se cree una obra derivada a partir del original.

Gradu Bukaerako Lanaren egileak, baimena ematen dio Mondragon Unibertsitateko Goi Eskola Politeknikoari Gradu Bukaerako Lanari jendeurrean zabalkundea emateko eta erreproduzitzeko; soiliik ikerketan eta hezkuntzan erabiltzeko eta doakoa izateko baldintzarekin. Baimendutako erabilera honetan, egilea nor den azaldu beharko da beti, eragotzita egongo da erabilera komertziala baita lan originaletatik lan berriak eratorzea ere.

Abstract

The aim of this project is to get accurate control of the most characteristic microstructure parameters to achieve a representative volume element (RVE) of AISI439 stainless steel. The study focuses mainly on the control of grain shape; however, grain size and orientation have also been taken into account. To achieve this, the characterization of the microstructure has been done based on electron backscatter diffraction measurements. The grain shape is characterised by the grain shape factor (also known as the aspect ratio) and tilt angle. DREAM3D has been used for the 3D RVE generation. In terms of the grain shape control, three different approaches have been used, i.e., equiaxed grains, elongated grain with the mean shape factor, and elongated grains with the shape factor distribution. The outputs of all three approaches have then been evaluated using microstructure representative assessment criterion and Kolmogorov-Smirnov testing methods. The final analyses of output RVE results have been done using MATLAB/MTEX. The program takes into account all the 2D section layers of the 3D RVE, which are summarized to get an overall view of the results. It is concluded that the elongated grain with the shape factor distribution input achieved the best control on grain shape performance. The final optimal RVE has shown a nearly perfect output result of the grain shape, i.e., grain shape aspect ratio and grain axis orientation as well as grain size. Besides, the texture performance meets the set standard.

Resumen

El objetivo principal de este proyecto es el control de las características más importantes de una microestructura y conseguir un elemento volumétrico representativo (RVE) del acero inoxidable AISI439. Este estudio se centra en el control de la forma de los granos; aun así, tiene en cuenta el tamaño y la orientación de los mismos. Para conseguir estos objetivos, la caracterización de la microestructura se ha hecho basándose en la medición hecha por el método de difracción de electrones por retrodispersión. La forma del grano se caracteriza mediante el factor de forma (también conocido como coeficiente de longitud) y grado de inclinación. Para la generación en 3D del RVE se ha utilizado el programa DREAM3D. Para controlar la variable de la forma de grano, tres diferentes métodos se han utilizado; la primera usando granos equiaxiales, la segunda usando granos alargados con el coeficiente de longitud media y la tercera usando granos alargados con la distribución de los coeficientes de longitud. Los resultados de las tres opciones han sido evaluados usando el método de evaluación de criterio de microestructuras representativas y el método de Kolmogórov-Smirnov. El análisis del RVE final se ha hecho usando MATLAB/MTEX. El programa tiene en cuenta todas las secciones 2D de la estructura y las combina para hacer un RVE en 3D, el cual permite tener una visión global de los resultados. Se ha concluido que el mejor método es el de los granos alargados con la distribución de los coeficientes de longitud. El RVE en 3D final demuestra tener unos resultados casi perfectos en lo que respecta a la forma de grano; tanto para el factor de longitud como para la orientación de los granos y para el tamaño. Asimismo, los resultados para la textura también cumplen los estándares requeridos.

Table of contents

Abstract	i
Resumen.....	ii
List of figures	v
List of tables	vii
1. Introduction	1
1.1. Background and problem statement	1
1.2. Objectives	1
1.3. Environmental and social impact	1
1.4. Work breakdown and time plan.....	2
2. Theoretical background.....	5
2.1. Microstructure features.....	5
2.1.1. Grain size	5
2.1.2. Grain shape.....	5
2.1.3. Grain orientation.....	6
2.2. Anisotropy	8
2.3. Microstructure modelling	9
2.4. Crystal plasticity modelling.....	9
3. Material	11
4. Experiments	13
4.1. Experimental procedures	13
4.2. Tensile properties	13
4.3. Microstructure characterization.....	15
4.3.1. The initial crystal microstructure.....	15
4.3.2. The initial crystal texture.....	18
4.3.3. The deformed crystal microstructure.....	19
4.3.4. The deformed crystal orientation.....	24
5. RVE generation with MRAC	31
5.1. General introduction	31
5.2. Size characterization control	31
5.3. Shape characterization control.....	33
5.4. Orientation characterization control	34
5.5. Evaluation.....	36
6. Development of MRAC	39
6.1. Introduction of post-process	39
6.2. Grain shape aspect ratio.....	40

6.3.	Grain tilt angle control.....	40
6.4.	Evaluation of distribution features	41
7.	CP model predictions	44
8.	Microstructure parametric study.....	45
8.1.	RVE with variant grain shape control	45
8.2.	RVE with variant grain axis orientation control.....	46
9.	Economic report	48
10.	Conclusions	49
11.	Future lines	50
12.	Personal evaluation of the traineeship	51
13.	References	52

List of figures

Figure 1: Thesis flow chart.....	4
Figure 2: Equivalent circle fitting for grain area [3].	5
Figure 3: Definition of major and minor axes in grain: red arrow marks the major axis, green arrow marks the minor axis, and β the grain shape orientation. (a): the measured original grain area; (b): equivalent ellipse method [3].	6
Figure 4: Cubic(a) and hexagonal (b) crystal structures [3].	6
Figure 5: Schematic illustration of the relationship between the crystal and specimen axes [5].	6
Figure 6: Schematic representation showing the Bunge definition of the Euler angles [4].	7
Figure 7: Presentation of the {100} poles of a cubic crystal in the stereographic projection. (a) Crystal in the unit sphere; (b) projection of the {100} poles onto the equator plane; (c) {100} pole figure and definition of the pole figure angles α and β for the (100) pole.[5]	7
Figure 8: ODF representation in 3D (a) and 2D (b) [2].	8
Figure 9: Work equivalence based conversion [9]	9
Figure 10: Scanning maps of AISI 439 sample from EBSD measurement: (a) the Auto-IQ map; (b) the ND-IPF map.....	12
Figure 11: Geometry of the tensile sample. All dimensions are in millimetre [9].	13
Figure 12: Engineering stress vs. engineering strain curves: for 0°, 45° and 90° (a) 15°, 30°, 60°, 75° (b); and true stress vs. true strain curves for 0°, 45°, and 90° (c) and 15°, 30°, 60° and 75°(d).	14
Figure 13: Yielding directionality of AISI439: yield stress (a) and normalized stress(b) at different loading angles.....	14
Figure 14: Experimental directional plastic strain ratio (r-value) in 0°,15°,30°,45°,60°,75° and 90° directions	15
Figure 15: R-values vs. true strain curves of different sample directions with respect to rolling direction (a) 0°,45°,90°; (b) 15°,30°,45°,60°,75°	15
Figure 16: Grain size distribution number fraction (a) and area fraction (b).	16
Figure 17: CDF graph for grain size experimental data vs. log-normal number fraction distribution fitting.....	16
Figure 18: Grain shape ratio distribution PDF (a) and CDF graphs (b)	17
Figure 19: Initial ODF figure with phi2=45° section.	18
Figure 20: Initial microstructure {100},{110},{111} pole figures.	19
Figure 21: Initial microstructure inverse pole figures.	19
Figure 22: Grain size for number fraction, area fraction and CDF graph for: 0 loading angle (a), 45 loading angle (b), 90 loading angle (c); 1: 10% strain rate, 2: 19% plastic strain	22
Figure 23: Grain size distribution at different plastic strain degree for loading direction angles of 0°, 45° and 90° with respect to RD.....	23
Figure 24: Grain shape aspect ratio evolution with different plastic strains and loading directions.....	24
Figure 25: CDF graph of grain shape aspect ratio evolution with different strain degrees and for different loading directions.....	24
Figure 26: Texture evolution for specimen at loading angle 0°. a:ODF figure at phi2=45°; b:{100},{110}, {111} pole figures; c: {110} inverse pole figures; 1: initial state; 2: after 10% deformation; 3: after 19% deformation.....	26
Figure 27: Texture evolution for specimen at loading angle 45°. a:ODF figure at phi2=45°; b:{100},{110}, {111} pole figures; c: {110} inverse pole figures; 1: initial state; 2: after 10% deformation; 3: after 19% deformation.....	28
Figure 28: Texture evolution for specimen at loading angle 90°. a:ODF figure at phi2=45°; b:{100},{110}, {111} pole figures; c: {110} inverse pole figures; 1: initial state; 2: after 10% deformation; 3: after 19% deformation.....	29

Figure 29: Grain size distribution with of grain shape distribution method compared to exp. data; 5 μm mesh size(a), 10 μm mesh size(b), 15 μm mesh size (c), and 20 μm mesh size (d); CDF (b); 1: bar-chart+PDF, 2:CDF graph.....	33
Figure 30: Grain shape with different mesh size.....	33
Figure 31: Grain shape effect with 10 μm mesh size and different approaches.....	34
Figure 34: ODF figures with phi2=45 of experiment data (a) and final RVE (b).	34
Figure 35: Pole figures of experimental data (a) and final RVE (b)	35
Figure 36: Inverse pole figures of experimental data (a) and final RVE (b).....	35
Figure 37: MRAD for output results of different grain shape distribution input methods with 10 μm mesh size.....	37
Figure 38: MRAD for mesh size effect on final RVE output results	38
Figure 39: Grain map of RVE, 2D (a) and 3D (b).....	39
Figure 40: 2D RVE fitting on ellipses disregarding edge grains. Pixels marked with yellow are disregarded.....	40
Figure 41: Experimental vs. final RVE grain shape aspect ratio results, bar chart+PDF (a) and CDP (b).40	
Figure 42: Grain axis orientation.....	41
Figure 43: Tilt angle input vs output values	41
Figure 44: Grain map of optimal RVE with the improved evaluation method	43
Figure 45: True stress-strain curve for CP simulation vs. other RVE configuration at different loading angles	44
Figure 46: Grains shape aspect ratio output data with input of 0.1(a), and 0.9 (b).	45
Figure 47: RVE generated with aspect ratio of, 0.1 (a), 0.5 (b), and 0.9 (c)	45
Figure 48:No tilt angle control vs. 45° input (a); 90° input; and 180° input	46
Figure 49: RVEs for grain tilt 45° (a), 90° (b) and 180° (c).....	47

List of tables

Table 1: Project planning	3
Table 2: The normal chemical composition of AISI 439 (mass content in %) defined in EN10088.....	11
Table 3: Grain number analysis.....	11
Table 4: Parameters of the lognormal distribution function fits on grain size	17
Table 5: Fitting parameters of beta distribution of grain shape.....	18
Table 6: Fitting parameters of diameter in μm for grain size distribution at different strain rates and loading angles.....	23
Table 7: Fitting parameters for grains shape aspect ratio at different plastic strain degree for different loading angles.....	24
Table 8: Texture index of orientation distribution function for the measured specimens.....	30
Table 9: Inputs for different shape control	31
Table 10: Mesh size effect grain size	33
Table 12: Experiment vs. output beta distribution orientation values for different mesh size.....	36
Table 13: Comparation of output parameters with different approaches with 10 μm mesh size.	37
Table 14: Comparation of microstructural data of intermediate RVE with different mesh sizes.	38
Table 15: Grain shape aspect ratio results for KS test.....	42
Table 16: Grain size and shape data of final RVE obtained by KS testing.....	42
Table 17: Numerical settings and microstructure features of the optimal RVE of AISI439.....	43
Table 18: Crystal plasticity parameters of AISI 439 calibration by polycrystal simulation with CPFFT at RT.....	44
Table 19: Cost of the project resources.....	48

1. Introduction

In this chapter the background, purpose and significance of the study are discussed.

1.1. Background and problem statement

For many years in the area of material science the different variables that affect the materials have been analysed such as grain size, shape and orientation. After many studies, it has been discovered that the control of said variables will help in the behaviour prediction. One of the main variables to be controlled during this process is the grain shape. The controlling of grain shape and orientation results directly improve the representative volume element (RVE) model results that are later used for making predictions of the stress-strain states simulations. The accurate control of this variable is not only of great importance in the area of material engineering but in the overall prediction of elastoplastic and fracture behaviour foresee of materials.

The outcome of this thesis shall be to control said variables in a way to get good prediction outcomes on various grain shape related aspects in order to further develop the generation of RVEs and to identify the current limitations for its control using Dream3D. Further explanation of the scope can be seen in Appendix A.

1.2. Objectives

The aim of this study is to investigate the effect of different approaches to control grain shape and its effect on the prediction of properties of a material.

The main objective of this study is to get further control on the grain shape variable to further make better predictions of the behaviour of the chosen material. For achieving this general objective, the following sub-objectives have been set:

- To achieve very good grain shape control via Dream3D with a minimal error.
- Achieve good control over grain size.
- See how the control of the grain shape axis can be done.
- Generate program to analyse grain parameters of final RVE.
- To create a structure model build-up with better representativeness of current models.

1.3. Environmental and social impact

In the current society where we live, in order to select a certain material with specific behaviour can be difficult due to the big selection of choices. Therefore, the only way to currently choose the perfect material is to do experiments with a big variety of different materials until the right one is chosen. In order to make this process faster, cheaper and more environmentally friendly ICME procedures are used.

Integrated computational materials engineering (ICME) has been intensively developed for the recent decade driven by production and process optimisation and new material development [1]. ICME is aimed at integrating all the available simulation tools into multiscale modelling strategies capable of simulating processing, microstructure, properties and performance of engineering materials, so new materials can be designed, tested and optimized before they are actually manufactured in the laboratory [2].

The working process of this method consists of firstly understanding how the microstructure of the material develops during processing and analysing the relationship between the microstructure and the properties. In order to generate this link, experiments are a vital part of the process to calibrate and validate the created models. Once the models are verified, it is possible to do predictions on the behaviour of the material without the need of experiments which helps in selecting the actual material for a given application.

This new virtual working method is very relevant specially for the customers, as the cost of the final product reduces drastically. Finding the right material with fewer experimental tries saves money for the producer resulting in a cheaper product. Moreover, its effect on the environment is also immense. The industry of today

wastes tons of energy and water to produce samples that are later thrown away. Therefore, this project is vital in order to further develop this working method and to get closer to achieving results in a cheaper way and with less effect on the environment.

1.4. Work breakdown and time plan

In order to achieve the set objectives first the description of the material must be done using experimental results obtained by the Electron Back-Scatter Diffraction (EBSD) method which is further analysed by MATLAB MTEX toolbox. The main aspects that are analysed are the grain size, shape and orientation. Following up using DREAM3D, these parameters, in specific the grain shape, are controlled, and the structure model is set up. After, the material's mechanical properties, anisotropic behaviour and microstructure evolution can be analysed in comparison with the experimental results.

In order to achieve the objectives in the set time, a work breakdown structure has been generated with the tasks and subtasks and its time plan.

- To complete the objectives stated previously, a series of tasks and sub-tasks have been set and a timeline has been defined to fulfil the project on time. This timeline has been defined by a Gantt chart. (See Table 1).
- a) Microstructure characterization
 - T1.1 Texture
 - T1.2 Grain size
 - T1.3 Grain shape
- b) RVE generation and evaluation
 - T2.1 Statistical microstructure characterization
 - T2.2 Grain size control
 - T2.3 Grain shape aspect ratio control
 - T2.4 Grain shape orientation control
- c) Improvement of RVE performance
 - T3.1 Post process on the final RVE structure
 - T3.2 Grain shape aspect ratio evaluation
 - T3.3 Grain shape orientation evaluation
 - T3.4 KS testing
- d) Documentation
 - T4.1 Report writing.
 - T4.2 Presentation

Table 1: Project planning

TASK	November	December	January	February	March	April	May	June
Microstructure characterization								
T1.1								
T1.2								
T1.3								
RVE generation and evaluation								
T2.1								
T2.2								
T2.3								
T2.4								
Improvement of RVE performance								
T3.1								
T3.2								
T3.3								
T3.4								
T3.5								
Documentation								
T4.1								
T4.2								

In order to achieve all of the objectives in the set time plan and to get a clear idea of the thesis workflow a flow chart has been made. (Figure 1).

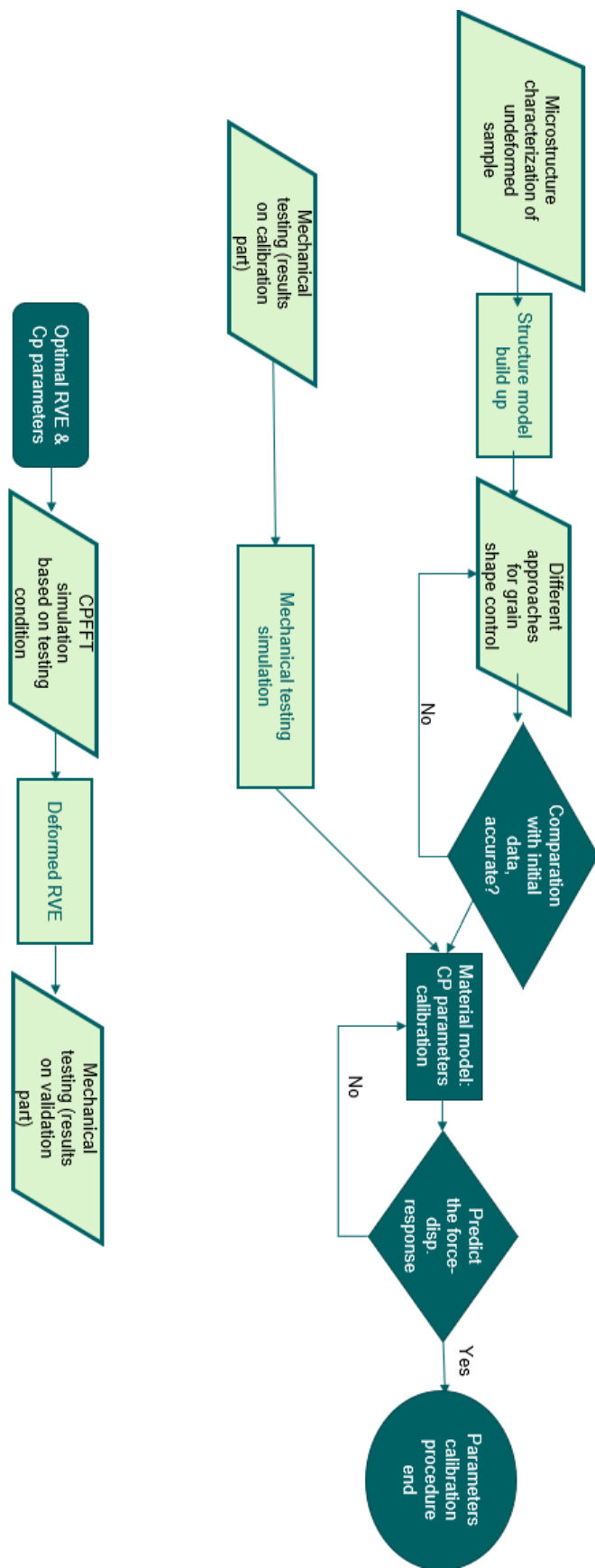


Figure 1: Thesis flow chart

2. Theoretical background

Relevant concepts for the completion of this thesis are presented in this section.

2.1. Microstructure features

The main features of a microstructure, the grain size, shape and orientation are going to be discussed in this chapter.

2.1.1. Grain size

In order to do a quantitative representation of the macroscopic properties, microstructural information has to be analysed, where one of the most important information is the characteristic length scale, i.e., the grain size (grain diameter). Crystalline solids are composed of grains of different sizes, which is represented by the grain size distribution. The most convenient and thus, most common is its derivation from optical micrographs by using the recognition of grain boundaries. The grain size distribution function is defined as the statistical frequency of specific grain sizes. The representative of the frequency of a particular characteristic based on intervals of a measure is referred to as histogram [3].

The grain size is characterized by fitting the equivalent diameter. In the case of 3D, the fitting of a sphere is done that gives the same equivalent volume as the initial grain, and in the case of 2D, the fitting of a circle with the same equivalent area is done. From each fitted figure, the equivalent diameter D is calculated to do the characterization of the grain size, as shown in Figure 2.

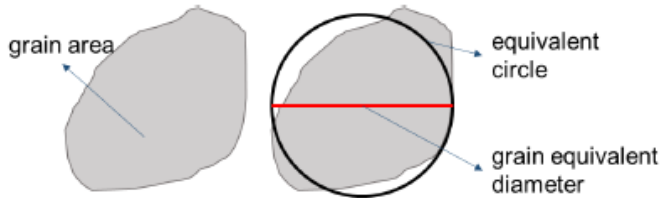


Figure 2: Equivalent circle fitting for grain area [4].

The size distribution of crystalline solids follows the logarithmic normal distribution. From this characterization, the most important values are the median value, mean value and standard deviation.

2.1.2. Grain shape

Grains with the same size may have different shapes and therefore lead to different behaviour, thus it is a very important characteristic for material microstructure.

Grains are usually elongated in one direction and therefore ellipses are used in other to do their fitting in case of 2D and ellipsoid in the case of 3D. This fitting is done by the aspect ratio between the shortest and the longest diagonals of the fitted ellipse. This data is then used for the grain shape factor distribution where all grain aspect ratios are represented in a histogram which usually follows a beta distribution.

In the case of 3-dimensional fittings, the grain shape is described as the length ratio of the three ellipsoid axes, i.e. a:b:c. For example, a:b:c=1:1:1 refers to equiaxed grains whereas a:b:c=1:0.1:0.1 refer to grains elongated along RD [5]. The grain shape aspect ratio is the shape factor to measure the grain shape, which is defined by the division between the minor axis and the major axis of the fitted ellipse, thus the values range from 0 to 1.

The second parameter is the grain shape orientation which is the angle between the major axis and the horizontal direction, shown in Figure 3.

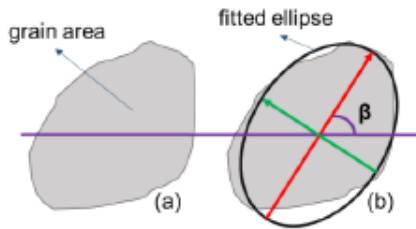


Figure 3: Definition of major and minor axes in grain: red arrow marks the major axis, green arrow marks the minor axis, and β the grain shape orientation. (a): the measured original grain area; (b): equivalent ellipse method [4].

2.1.3. Grain orientation

In this chapter, a brief overview of the definition of texture and grain orientation distribution characterization is done. The two main techniques used for this analysis are the X-ray diffraction (XRD) method and the EBSD method with scanning electron microscopy (SEM).

2.1.3.1. Crystallographic orientation definitions

Most solid-state materials, including metals, ceramics, and minerals, have a polycrystalline structure that is composed of a multitude of individual crystallites or “grains” [6]. Materials whose constituents are arranged in highly ordered and repeating patterns in all three directions are called crystalline solids which mostly crystallize in either hexagonal or cubic structures (Figure 4).

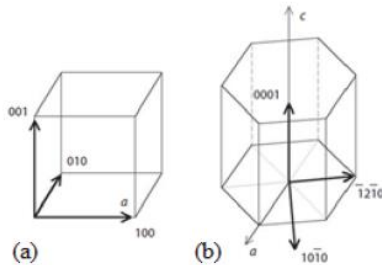


Figure 4: Cubic(a) and hexagonal (b) crystal structures [3].

The texture is the preferred grain orientation distribution, which is a combination of three variables that specify the orientation of the crystal structure regarding the axes of the specimen. Texture plays a great role in the anisotropy and behaviour of the material and its properties depend on the crystallographic direction in which it is measured.

The axes of the specimen system are chosen according to the directions associated with the external shape of the specimen. The most common directions associated with the external shape are the rolling direction (RD); the through-thickness direction, which is the normal direction to the rolling plane (ND); and the transverse direction (TD), as illustrated in Figure 5.

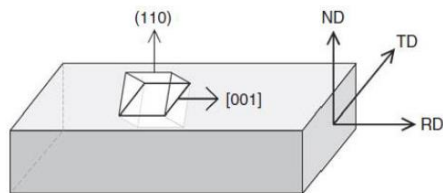


Figure 5: Schematic illustration of the relationship between the crystal and specimen axes [6].

The most common way to represent orientation is the Euler angle method as it only uses three rotations: $\varphi_1, \Phi, \varphi_2$. There are several definitions used to define Euler angles but in this thesis, the Bunge definition [7] is applied (Figure 6).

- 1. Rotation: φ_1 about the ND, transforming the rolling direction RD into RD', on (001) plane of the crystal frame and TD into TD'.
- 2. Rotation: Φ about the axis RD' (in its new orientation), transforming the normal direction ND into direction [001] of the crystal frame and bringing TD into the (001) plane in the crystal frame.
- 3. Rotation: φ_2 about ND'' (in its new orientation, i.e. [001] direction).

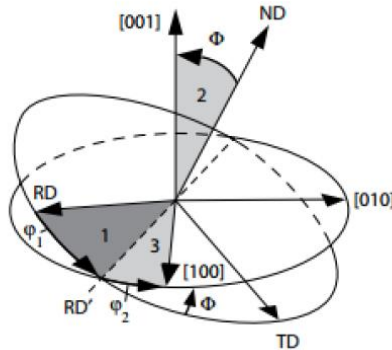


Figure 6: Schematic representation showing the Bunge definition of the Euler angles [4].

2.1.3.2. Characterization of grain orientation distribution

In order to characterize the texture of a microstructure three figures are used: pole figure (PF), inverse pole figures (IPF) and orientation distribution functions (ODF).

Pole figures are used to provide a graphical representation of orientation and are measured by X-ray texture goniometer or EBSD method.

A pole figure is a two-dimensional graphical representation of orientation, showing the orientation of the selected plane normal (a pole) with respect to the sample reference frame. This pole vector in a three-dimensional space and is imagined as a hemisphere surrounding a crystal unit cell. The pole intersects the hemisphere at a three-dimensional point and this intersection location is projected into a two-dimensional plane using the stereographic projection method [8]. This method is represented in Figure 7.

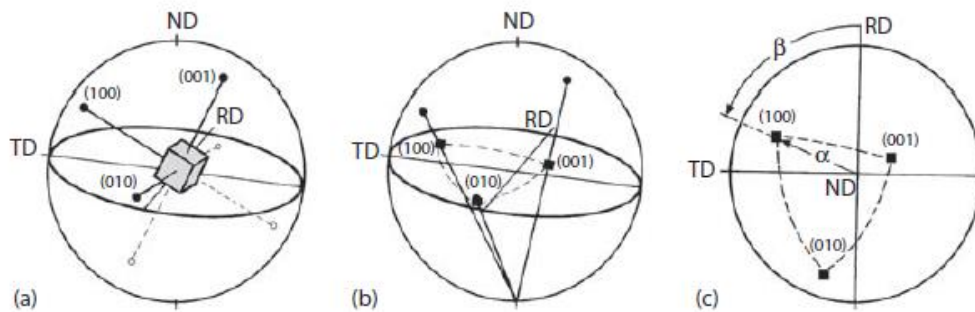


Figure 7: Presentation of the {100} poles of a cubic crystal in the stereographic projection. (a) Crystal in the unit sphere; (b) projection of the {100} poles onto the equator plane; (c) {100} pole figure and definition of the pole figure angles α and β for the (100) pole.[6]

Secondly, inverse pole figures are a complement for pole figures. Rather than representing the orientation of the crystal coordinate system in the specimen coordinate system, they represent the orientation of the specimen coordinate system projected into the crystal coordinate system. Therefore, the reference system of the

inverse pole figure is the crystal coordinate system, and the “orientation” is defined by the axes of the specimen coordinate system, for example, RD, TD, and ND [6].

The third parameter is the orientation distribution function. It associates the orientation of each grain of a certain volume with other crystals in a polycrystalline specimen that has the same orientation. Therefore, it is a probability density function of orientations.

It is represented in the orientation space, where each orientation is given by a point. The orientation of a crystal can be described in terms of the orientation of its cell, i.e., the orientation of its crystal coordinate system with regard to the specimen coordinate system. To make the crystal coordinate system coincide with the specimen coordinate system a rotation must be done using the three Euler angles. To display the intensity distribution of each section, lines of equal intensity are used (Figure 8).

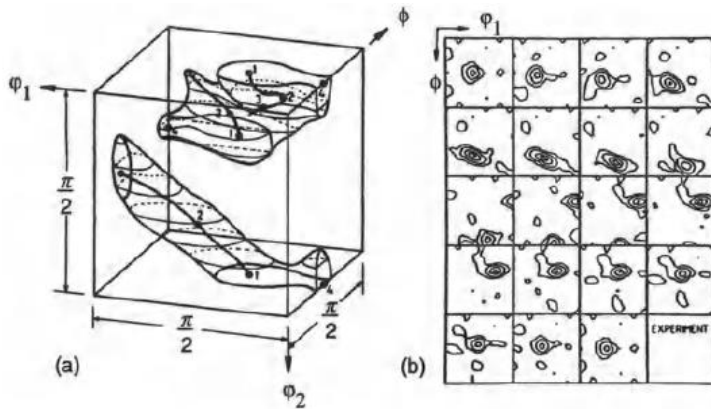


Figure 8: ODF representation in 3D (a) and 2D (b) [3].

2.2. Anisotropy

Anisotropy is the quality of exhibiting properties with different values when measured along different directions. Anisotropy is most easily observed in single crystals of solid elements or compounds, in which atoms, ions or molecules are arranged in regular lattices [9]. This difference in the properties is especially seen in materials that undergo rolling processes. The anisotropic behaviour means materials exhibit different stress-strain curves when tested along different directions. In order to compare the stress-strain curves from different specimens, the data must be converted using the work equivalent principle, as shown in Figure 9.

Θ is the angle between the loading direction and the rolling direction of the material. The equivalent plastic strain $\bar{\varepsilon}^P$ (PEEQ) is determined by equalling the integral area of the Θ degree flow curve at ε_0^P and the rolling direction flow curve at PEEQ. The equivalent plastic stress $\bar{\sigma}_\Theta$ is now transferred to the PEEQ point and the combination of all new PEEQ and plastic stress points constitutes the new work equivalent flow curve [10][11].

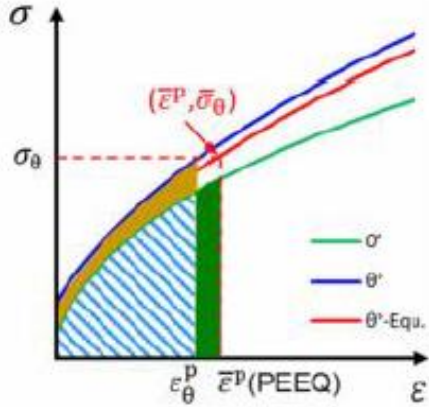


Figure 9: Work equivalence based conversion [9]

Another measurement for characterizing the material is the r-value or Lankford coefficient which defines the ratio increment of the true plastic strain of width (ε_y^p) and the true plastic strain of thickness (ε_z^p) of the tested sample [12]. High R-values indicate good formability in sheet forming operations; whereas low R-values indicate rapid sheet thinning and premature failure.

2.3. Microstructure modelling

For understanding and defining the relation of the microstructural features of a material with its plasticity, damage and fracture behaviour, microstructural numerical models are usually used [3]. In the last years, several approaches to microstructure-based modelling have been developed, like molecular dynamics or Monte Carlo method for the descriptions of atomic-level properties, dislocation dynamics for dislocation motion modelling and crystal plasticity (CP) for the crystal and phase scale modelling. For microstructure representation, representative volume element, statistical volume element (SVE) or uncorrelated volume element (UVE) can be used [44]. Of all these approaches, the current study focuses on a combination of RVEs and CP formulation.

An RVE is defined as “the smallest material volume element of the composite for which the usual spatially constant (overall modulus) macroscopic constitutive representation is a sufficiently accurate model to represent the mean constitutive response” [24]. RVE models are generated either by real microstructure or by statistically characterized synthetic microstructure [25] and can be 2-dimensional planar or 3 dimensions.

2.4. Crystal plasticity modelling

The crystal plasticity model and the equations used in DAMASK are based on the dislocation slip mechanism theory [13]. The constitutive model gives the relation between the deformation gradients with the stresses without considering the dislocation density.

The deformation gradient \mathbf{F} can be decomposed in elastic deformation gradient \mathbf{F}_e and plastic deformation gradient \mathbf{F}_p (Equation 1):

$$\mathbf{F} = \mathbf{F}_e \mathbf{F}_p \quad (1)$$

The derivation of the plastic deformation gradient $\dot{\mathbf{F}}_p$ rate is expressed in equation 2:

$$\dot{\mathbf{F}}_p = \mathbf{L}_p \mathbf{F}_p \quad (2)$$

where \mathbf{L}_p is the plasticity velocity gradient. \mathbf{L}_p is dependent on the shear rates on all the slip systems. If the deformation process involves only dislocation slip, \mathbf{L}_p is defined as equation 3:

$$\mathbf{L}_p = \sum_{\alpha=1}^N \dot{\gamma}^\alpha \mathbf{m}^\alpha \otimes \mathbf{n}^\alpha \quad (3)$$

where α is a slip system, $\dot{\gamma}^\alpha$ is the slip shear rate, \mathbf{m}^α is the unit vector along the shear direction, \mathbf{n}^α is the unique vector along the shear plane normal and N is the number of active slip systems. The shear rate $\dot{\gamma}^\alpha$ is determined by the resolved shear stress τ^α and the critical resolved shear stress τ_c^α . The kinetic law on the slip system α is given by equation 4:

$$\dot{\gamma}^\alpha = \dot{\gamma}_0 \left| \frac{\tau^\alpha}{\tau_c^\alpha} \right|^m \operatorname{sgn}(\tau^\alpha), \quad (4)$$

where, $\dot{\gamma}_0$ is the reference shear rate and m the rate sensitivity of slip α . The resolved shear stress τ^α on slip system α is defined by equation 5:

$$\tau^\alpha = \mathbf{S} \cdot (\mathbf{m}^\alpha \otimes \mathbf{n}^\alpha), \quad (5)$$

where \mathbf{S} is the second Piola-Kirchhoff stress in the intermediate configuration defined by \mathbf{F}_e . The micromechanical interaction between different slip systems is determined by equation 6:

$$\dot{\tau}_c^\alpha = \sum_{\beta=1}^N h_{\alpha\beta} |\dot{\gamma}^\beta|, \quad (6)$$

where $h_{\alpha\beta}$ is the hardening matrix is given by equation 7:

$$h_{\alpha\beta} = q_{\alpha\beta} \left[h_0 \left(1 - \frac{\tau_c^\beta}{\tau_c^s} \right)^\alpha \right], \quad (7)$$

where h_0 , α , and τ_c^s are the slip hardening parameters. $q_{\alpha\beta}$ defines the effect of self-hardening ($\alpha = \beta$) and latent hardening ($\alpha \neq \beta$). Finally, the hardening law of the slip system α is defined by equation 8.

$$\tau_c^\alpha = \tau_0 + \int_0^t q_{\alpha\beta} \left[h_0 \left(1 - \frac{\tau_c^\beta}{\tau_c^s} \right)^\alpha \right] |\dot{\gamma}^\beta| dt, \quad (8)$$

where τ_0 is the initial critical resolved shear stress.

3. Material

The material used in this study is AISI349, a ferritic stainless steel, stabilized with titanium, 16-18 percent chromium alloyed and low carbon steel with very good resistance to intergranular and pitting corrosion. Its chemical composition, shown in Table 2, provides it with good weldability due to the titanium stabilization and has excellent resistance to stress corrosion cracking, high thermal conductivity, and low thermal expansion. These properties make it perfect to use in heat exchangers, hot water tanks and automotive exhaust system components. Moreover, its reflective colour and fabricability have resulted in its use for small diameter tubes to replace solid wire spokes in automotive wheel cover applicators [14].

Table 2: The normal chemical composition of AISI 439 (mass content in %) defined in EN10088.

C	Si	Mn	P	S	Cr	Ti	Ni
≤ 0.05	≤ 1.00	≤ 1.00	≤ 0.04	≤ 0.015	16.0-18.0	0.15 -0.80	≤ 0.30

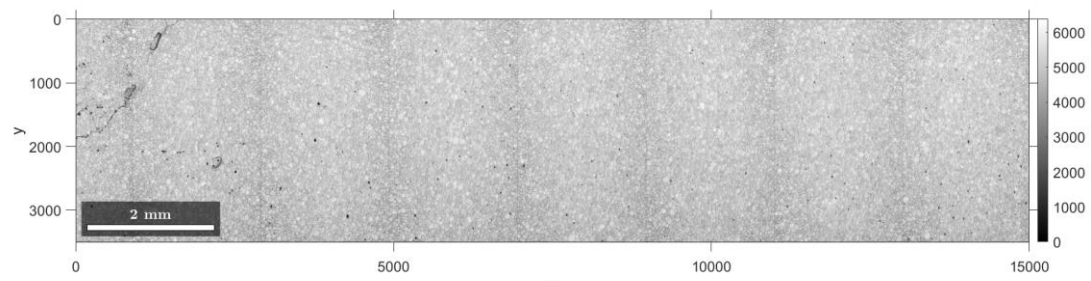
As for the microstructure, AISI439 is a ferritic, body-centred crystal structured at all temperatures below the melting point. EBSD is used to analyse the texture and microstructure of the as-delivered material (Figure 10). The measured sample size is 3.5 mm×15 mm and the scanning space is 5 μm.

The grain reconstruction and analysis are carried out by using the software MATLAB/MTEX. With the aim to obtain the best results, the grain boundary reconstruction has been analysed with 5 and 15 degrees, meaning that the minimum misorientations between two scatter points are 5 and 15 degrees respectively. First, the number of alpha grains is counted and then the grains located at the edges are disregarded as they are cut and therefore are not representative. After doing this analysis the number of grains achieved is the following (Table 3):

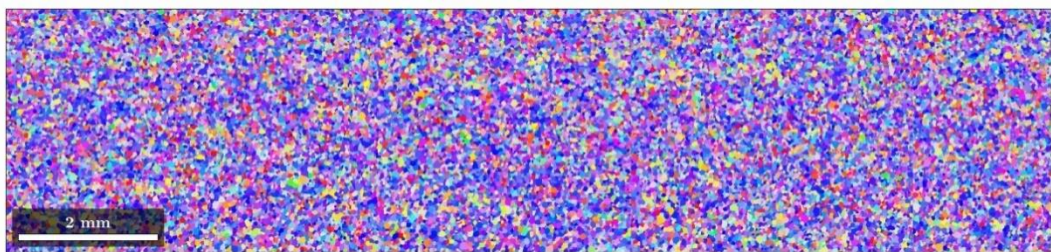
Table 3: Grain number analysis

	5 degrees	15 degrees
Initial number of grains	43089	31457
Alpha grains	40900	30027
Inner grains	39815	29060
Outer grains	1085	967

For further analysis, the data obtained from 15° misorientation has been used as it is a high angle grain boundary criterion, which is needed to distinguish the inner substructure of the grains and provides enough grains to do a representative analysis.



(a)



(b)

Figure 10: Scanning maps of AISI 439 sample from EBSD measurement: (a) the Auto-IQ map; (b) the ND-IPF map

4. Experiments

In this section, how the material testing is done is explained. The results of this tests have been taken from literature. Uniaxial tensile tests are done to investigate the mechanical properties, and EBSD measurements are used for the microstructure and texture characterization.

4.1. Experimental procedures

In the uniaxial test, the specimen of AISI439 is subjected to deformation at a quasi-static strain rate and room temperature using a universal tensile test machine (Zwick 100kN) until it fractures, as described in European Standard EN 10002-1 [10]. The applied load and extension are measured by means of a load cell and strain gauge extensometer of 50 mm, respectively. The geometry and dimension of the sample are shown in Figure 11.

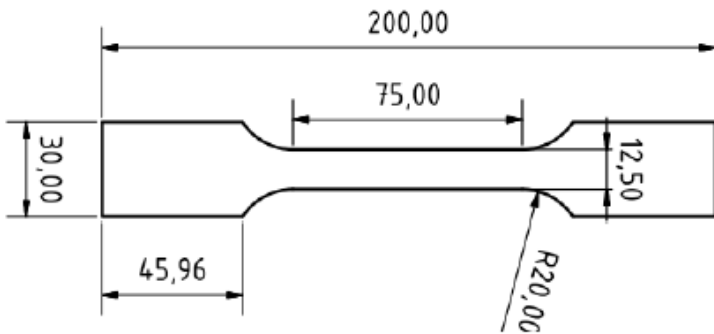


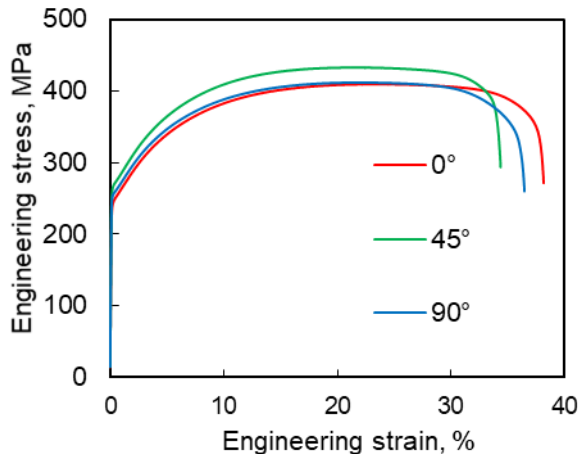
Figure 11: Geometry of the tensile sample. All dimensions are in millimetre [10].

Moreover, and in order to determine the flow behaviour and the planar anisotropy of the material, seven different loading directions ($0^\circ, 15^\circ, 30^\circ, 45^\circ, 60^\circ, 90^\circ$) with respect to the specimen rolling direction are tested under the stain rate of $2.7 \times 10^{-4} s^{-1}$.

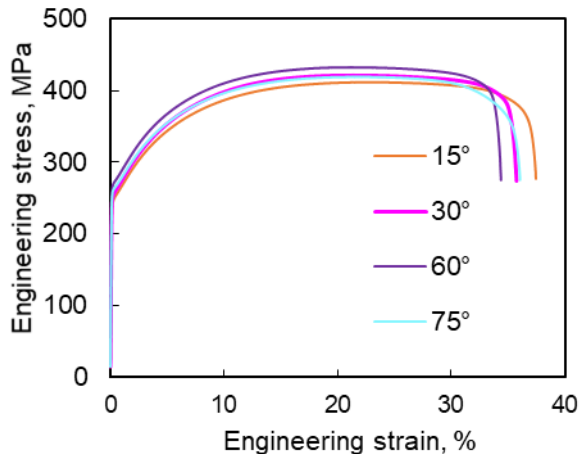
In addition, to investigate the texture evolution during plastic deformation, the uniaxial tensile test is conducted at room temperature and a strain rate of $2.7 \times 10^{-4} s^{-1}$ for three loading angles ($0^\circ, 45^\circ$ and 90°) with respect to the loading direction. Each group has two specimens with true stains of 0.1 and 0.19.

4.2. Tensile properties

The engineering and true stress-strain curves of AISI439 with different loading angles are shown in Figure 12. The yield stress is not uniquely defined because of the continuous transition from the elastic to plastic range.



(a)



(b)

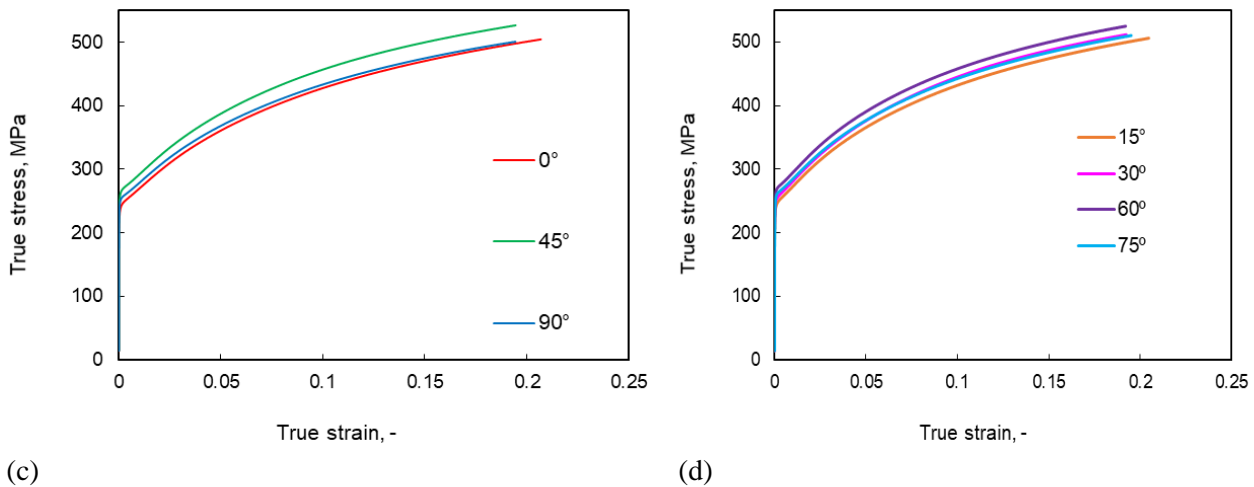


Figure 12: Engineering stress vs. engineering strain curves: for 0°, 45° and 90° (a) 15°, 30°, 60°, 75° (b); and true stress vs. true strain curves for 0°, 45°, and 90° (c) and 15°, 30°, 60° and 75°(d).

Figure 13 shows the materials yielding point Rp0.2 for different loading directions and the normalized yield stresses with respect to the one loaded along RD. This stress is where the remaining plastic strain would be 0.2%.

The normalized yield stress has a maximum at the loading angle of 60° and a second maximum at the loading angle of 45° with a very similar value. From these two values on, it decreases progressively reaching its lowest value at 0° loading angle. From these responses, the significant anisotropy in strength and uniform strain can be noticed.

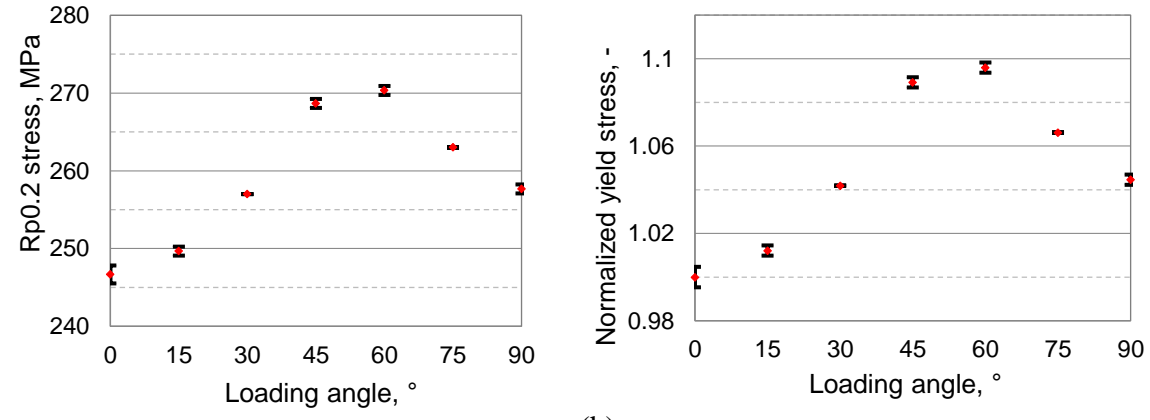


Figure 13: Yielding directionality of AISI439: yield stress (a) and normalized stress(b) at different loading angles.

The r-value or Lankford coefficient refers to the measure of anisotropy during the plastic deformation of sheets. This is normally measured at 20% of the engineering stress in tensile tests. Texture has a great influence on Lankford's coefficient and therefore a small change in the input leads to a big difference in R-values. While deformation is progressed, the change of normalized stress can be attributed to the evolution of the texture during deformation.

In Figure 14, it can clearly be seen that the r-value varies depending on the loading angle which indicates this sample has in-plane anisotropy [15]. It reaches the minimum point at the loading angle of 45° with respect to the RD and increases progressively from 45° to RD and TD, then reaches the maximum point at the loading angle of 90°, i.e., the transverse direction. This slight asymmetry can be attributed to the presence of some texture components [16].

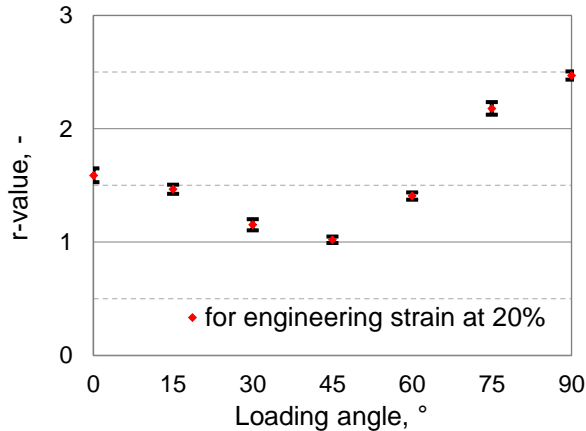


Figure 14: Experimental directional plastic strain ratio (r-value) in $0^\circ, 15^\circ, 30^\circ, 45^\circ, 60^\circ, 75^\circ$ and 90° directions

In terms of r-value evolution, it changes rapidly during the initial stages of straining and almost keeps constant after experiencing the true tensile strains as seen in Figure 15. In general, r-value has a small, reduced tendency for $0^\circ, 15^\circ$ and 30° loading angles, an increasing trend for the loading angle of $60^\circ, 75^\circ$ and 90° . The r-value of the loading angle 45° almost keeps constant during the entire deformation process. This change can be attributed to the evolution of the texture during deformation.

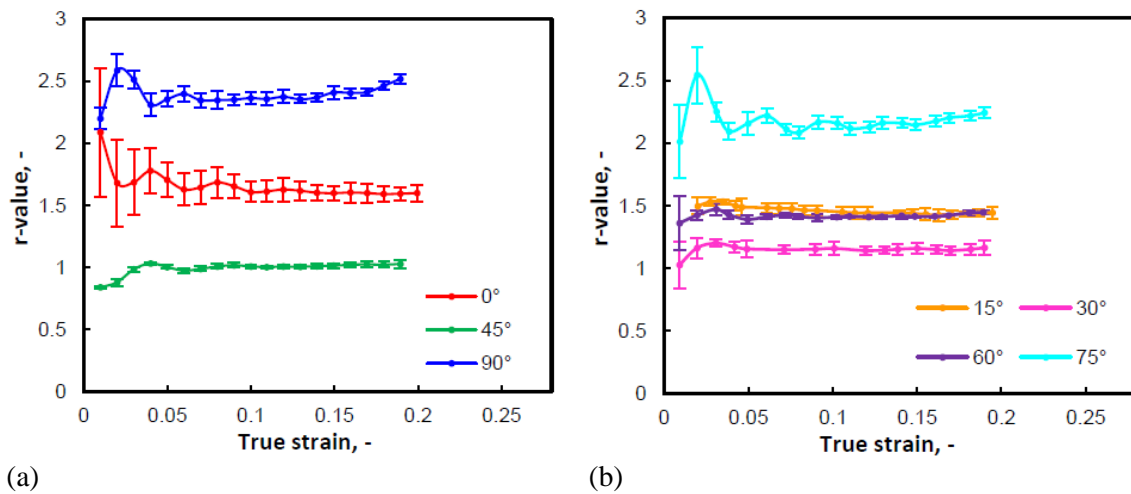


Figure 15: R-values vs. true strain curves of different sample directions with respect to rolling direction (a) $0^\circ, 45^\circ, 90^\circ$; (b) $15^\circ, 30^\circ, 45^\circ, 60^\circ, 75^\circ$.

4.3. Microstructure characterization

In order to compare the effect that grain shape control has in the final RVE generation, first the grain size distribution, grain shape distribution and texture of the input material have been analysed.

4.3.1. The initial crystal microstructure

Starting with the grain size distribution, the statistical frequency of specific grain size can be described by the number fraction or the area fraction. The two distributions obtained by the MATLAB fitting of the EBSD data are shown in Figure 16 and Figure 17. It can be seen that both distributions follow a logarithmic normal distribution, defined by the following mathematic equation (See equation 9).

$$f(d; \mu, \sigma) dy = \frac{1}{d\sigma\sqrt{2\pi}} \exp\left(-\frac{(lny-\mu)^2}{2\sigma^2}\right) dy, \quad (9)$$

where f is the probability density function.

The mode defines the y value at which the probability density function has a locally maximum value (Equation 10):

$$mode(y) = \exp(\mu - \sigma^2) \quad (10)$$

The mean value of the whole data is (see Equation 11):

$$mean(y) = \exp(\mu + \sigma^2/2) \quad (11)$$

The median is the value separating the higher half from the lower half of the data sample, i.e., where the cumulative value is 0.5 (Equation 12)

$$median(y) = \exp(\mu) \quad (12)$$

The standard deviation of the log-normal distribution is defined by Equation 13.

$$(13)$$

$$\sqrt{V} = \sqrt{\exp(2\mu + \sigma^2)(\exp(\sigma^2) - 1)}$$

The grain area fraction against grain size distribution makes the distribution more accurate as a correction with weights is done. When doing the analysis MATLAB gives many different characterized diameters, i.e., mean, mode, median values and the standard deviations for each kind of grain size distribution which are listed in Table 4. According to the literature, the mean value and standard deviation of grain size distribution with grain area fraction are chosen as the representative parameters for the grain size distribution for AISI 439 [4].

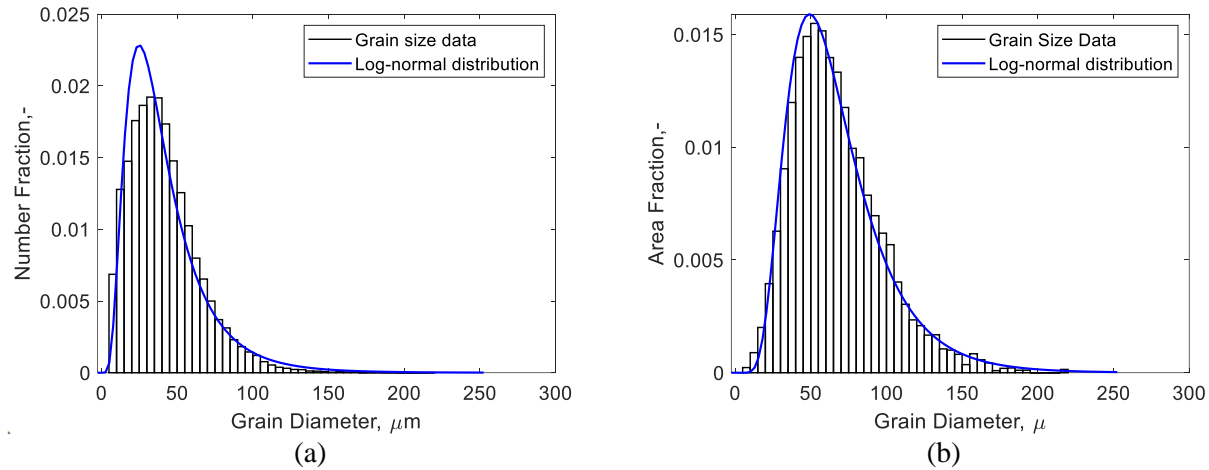


Figure 16: Grain size distribution number fraction (a) and area fraction (b).

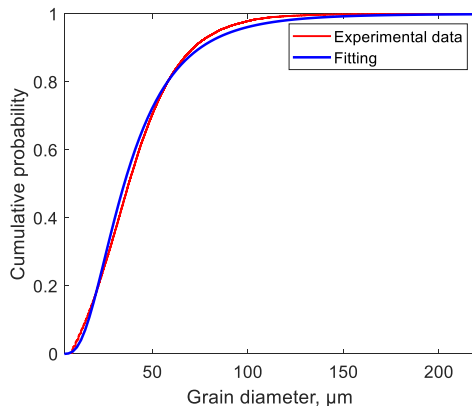


Figure 17: CDF graph for grain size experimental data vs. log-normal number fraction distribution fitting.

Table 4: Parameters of the lognormal distribution function fits on grain size

	Grain size fitting parameters (μm)			
	Mode value	Median value	Standard deviation	Mean value
Area fraction distribution	49.18	60.72	32.67	67.46
Number fraction distribution	24.89	35.23	27.03	41.92

On the other side, in what it refers to the grain shape characterization, the shape factor, i.e., aspect ratio, follows a beta distribution fitting described in Equation 14, 15 and 16.

$$f(x; \alpha, \beta) = \frac{1}{B(\alpha, \beta)} x^{\alpha-1} (1-x)^{\beta-1} \quad (14)$$

$$B(\alpha, \beta) = \int_0^1 x^{\alpha-1} (1-x)^{\beta-1} dt \quad (15)$$

$$\text{mean } (x) = \frac{1}{1 + \frac{\beta}{\alpha}} \quad (16)$$

The fitting of the experimental data is shown in Figure 18. Dream3D can only take as input the number fraction distribution and therefore only that one is analysed. The fitting parameters of the distribution made with MATLAB are listed in Table 5. Grain shape aspect ratio refers to the ratio of length between the minor axis and the major axis of the fitted ellipse grain. The three representative lengths of the three ellipsoidal axes along RD, TD, and ND are represented as a, b and c with the average grain shape aspect ratio being: b:a=0.7443, c:a=0.7204, i.e., a:b:c=1:0.7443:0.7204. Moreover, from the beta distribution fitting the mean values of the longest axis fitted ellipse, called alpha, and the length of the shortest ellipse, beta are obtained, 4.7362 and 1.6271 respectively.

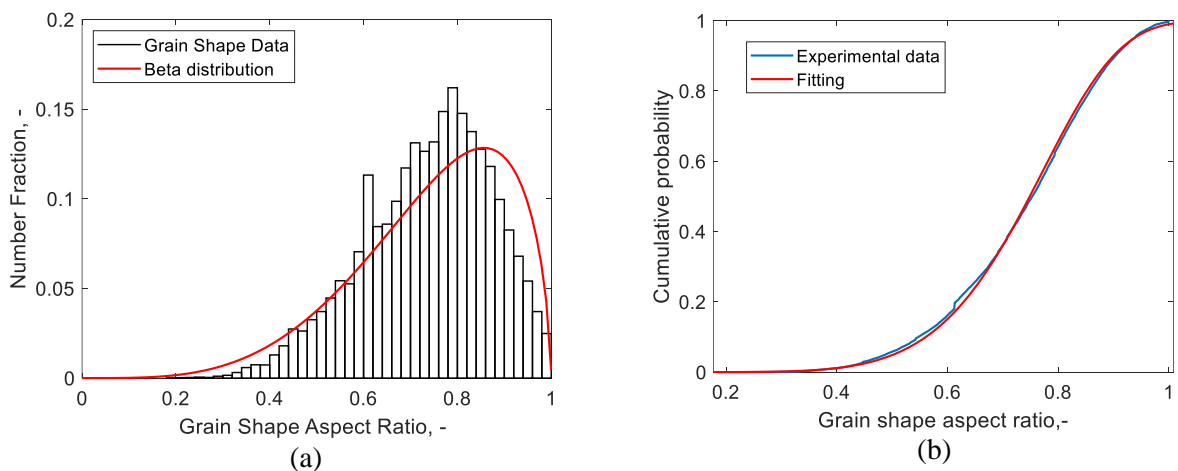


Figure 18: Grain shape ratio distribution PDF (a) and CDF graphs (b)

The parameters to fit the beta distribution are gathered in Table 5.

Table 5: Fitting parameters of beta distribution of grain shape.

Grain shape aspect ratio fitting parameters RD-TD plane		
Median value	Standard deviation	Mean value
0.7709	0.1607	0.7443

4.3.2. The initial crystal texture

The third aspect of the material that has been analysed is its texture. As it has been explained before, texture refers to the preferred crystal orientation. All the analysis of simulation results is done using MTEX and therefore the experimental texture processing initially done by EBSD are re-analysed using MTEX to be consistent with the results and to make representative comparations.

The process has various steps and the first one is to perform the grain reconstruction to obtain the ODF figures (Figure 19), pole figures (Figure 20) and inverse pole figures (Figure 21). The ODF is calculated by the kernel function with the Fourier-type series expansion method using the parameter half width=4.2°. Besides, the crystal symmetry is set as cubic and the specimen symmetry as orthorhombic.

The texture index is the variable that defines how strong or weak this texture distribution is. The increase of this texture index means the appearance of a fibre or component. In this case, the appearance of the γ fibre can be seen in the ODF.

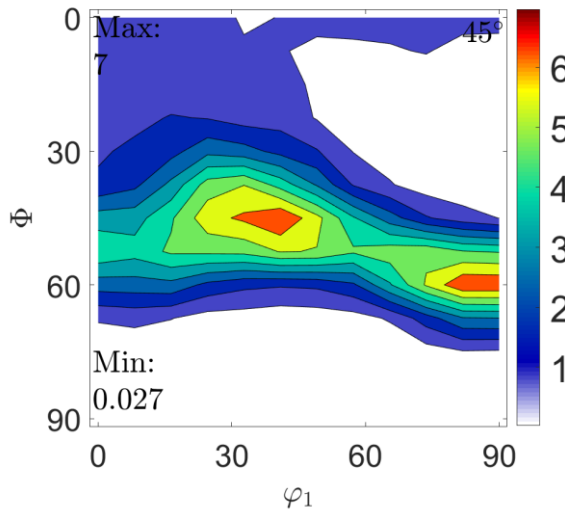


Figure 19: Initial ODF figure with $\phi_2=45^\circ$ section.

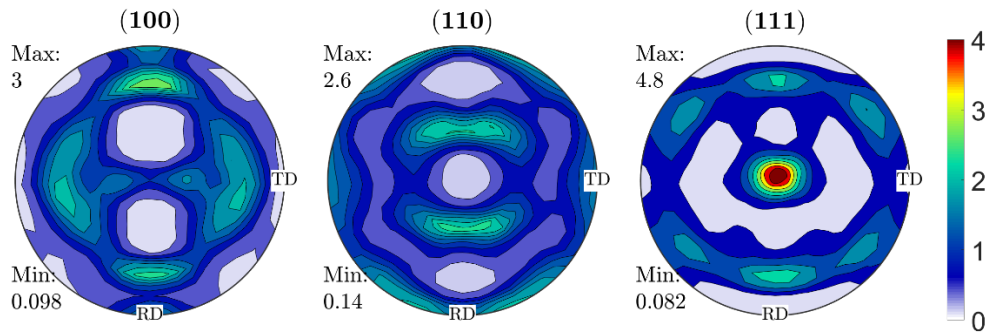


Figure 20: Initial microstructure $\{100\}, \{110\}, \{111\}$ pole figures.

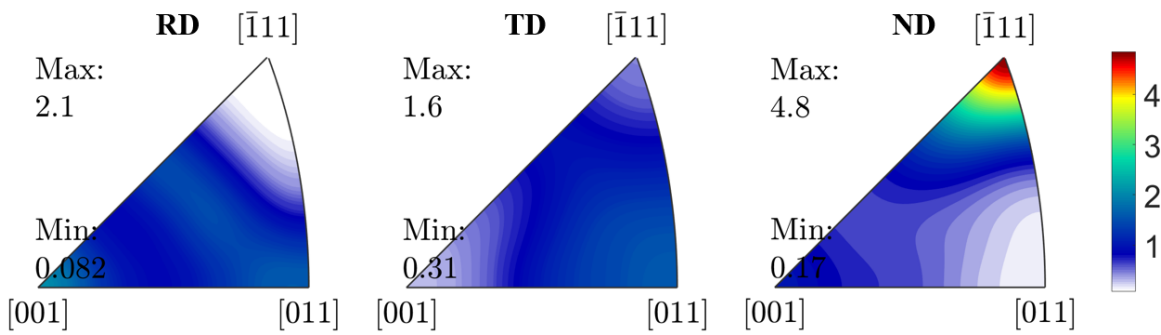
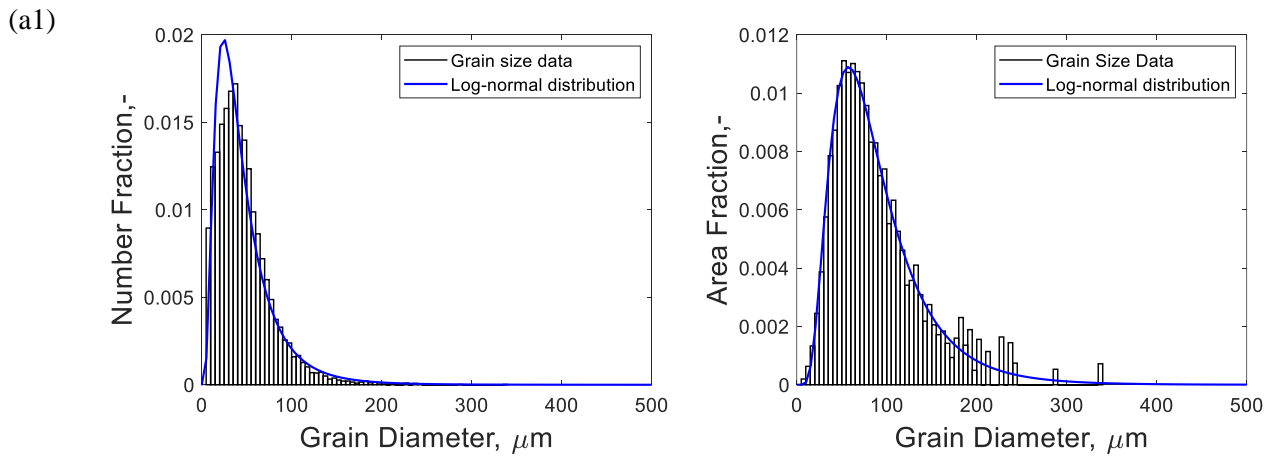


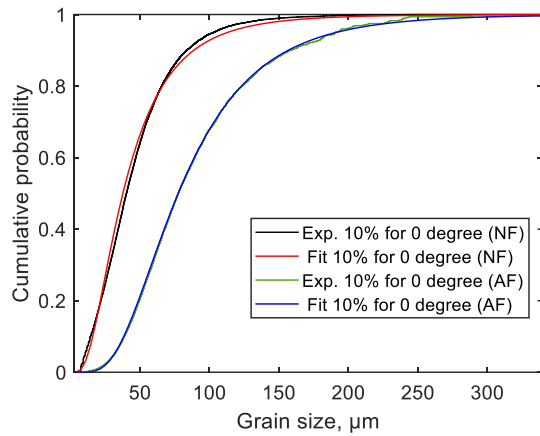
Figure 21: Initial microstructure inverse pole figures.

4.3.3. The deformed crystal microstructure

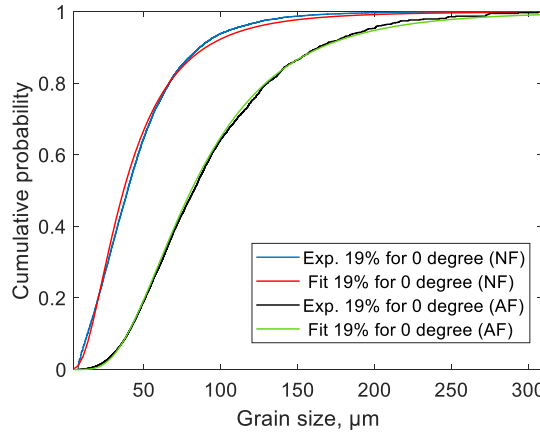
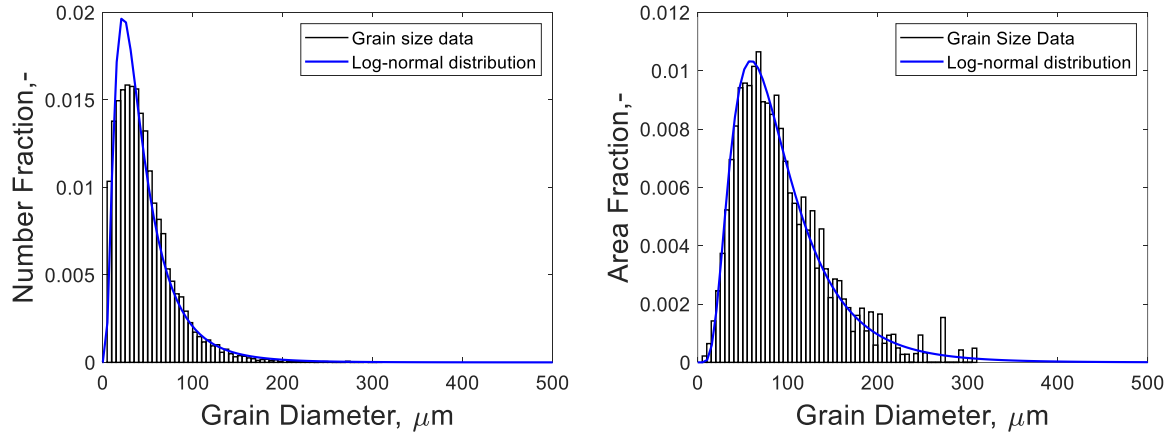
The grain size distribution evolution during deformation with different loading angles (0° , 45° and 90°) and plastic strain of 10% and 19%.

The grain size distributions for all the different loading angles and plastic strains with the proper fitting are shown in Figure 22.

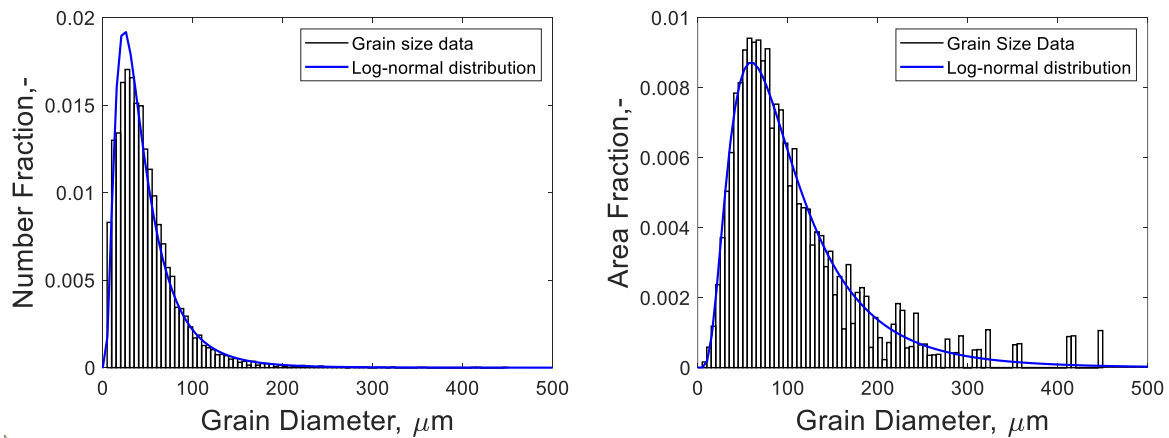


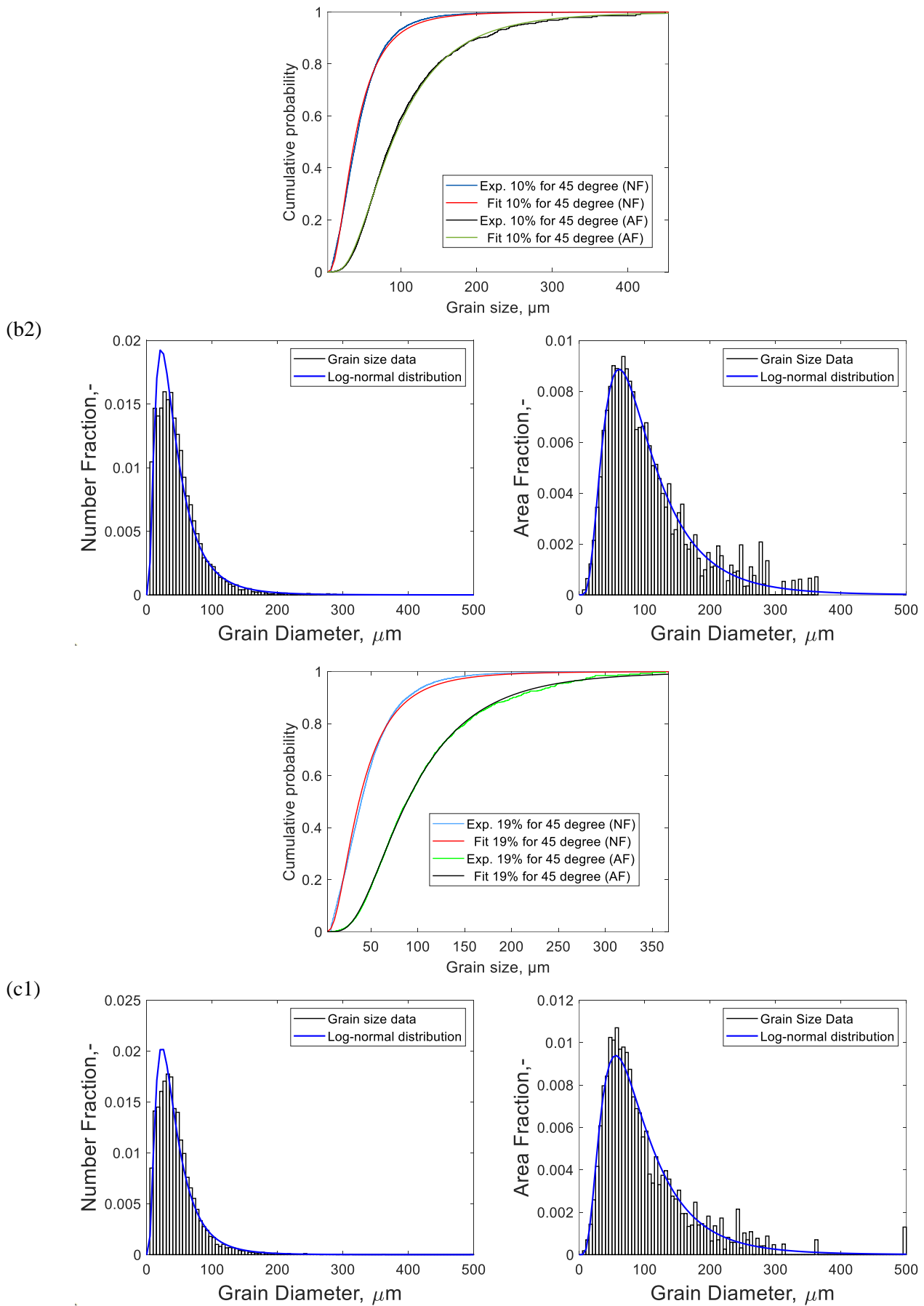


(a2)



(b1)





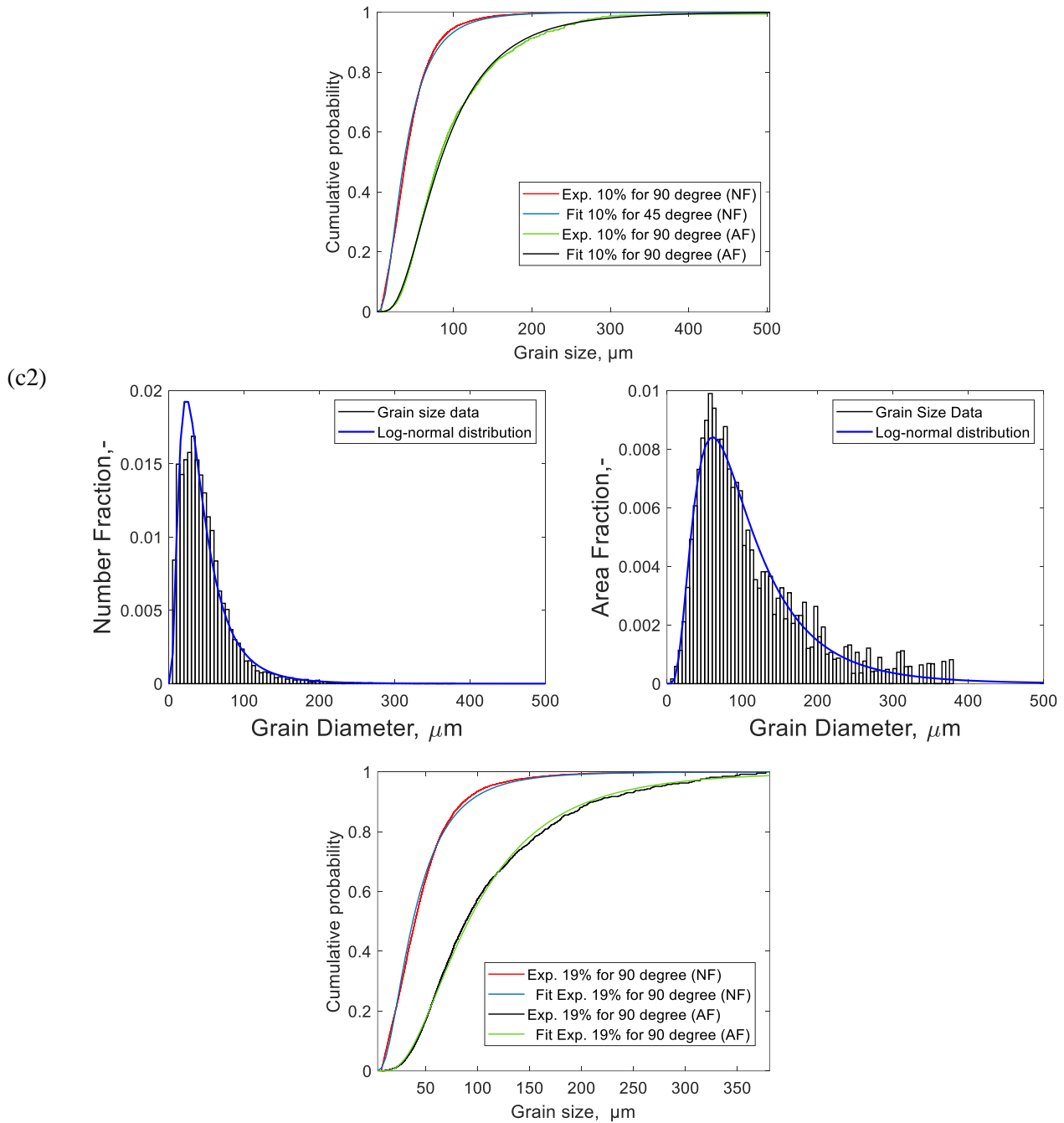


Figure 22: Grain size for number fraction, area fraction and CDF graph for: 0 loading angle (a), 45 loading angle (b), 90 loading angle (c); 1: 10% strain rate, 2: 19% plastic strain

The results show an overall perfect fit of the data for all of the cases.

Besides, the increase of the standard deviations represents an increase of the discrete degree in the grain size distribution, which means, plastic deformation leads to a more uneven distribution of grain size. The comparation of all the curves is shown in Figure 23.

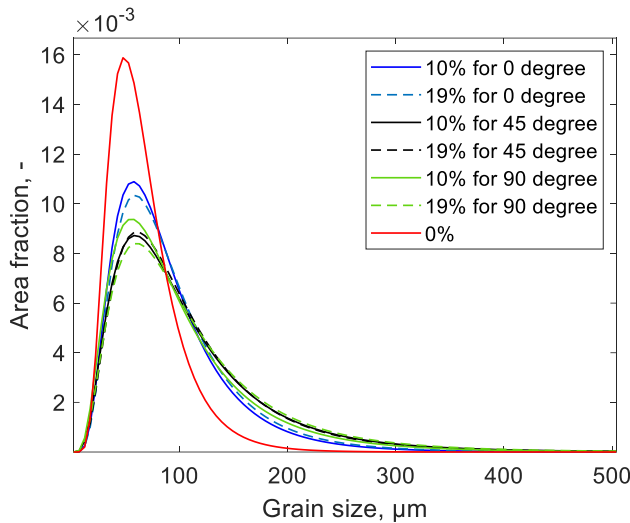


Figure 23: Grain size distribution at different plastic strain degree for loading direction angles of 0° , 45° and 90° with respect to RD.

All the specific fitting parameters for each case are gathered in Table 6. In general, the average grain size increases as the plastic deformation degree increases. This increase is given rapidly from the strain rate of 0% to 10%, yet the increase is lower from 10% strain rate to 19% strain rate. Furthermore, the standard deviation increases with plastic deformation, meaning that it creates a more uneven distribution of grain size.

Table 6: Fitting parameters of diameter in μm for grain size distribution at different strain rates and loading angles.

	Mean value			Standard deviation		
	0°	45°	90°	0°	45°	90°
0%	67.46			32.67		
10%	90.12	107.9	100.4	53.47	75.49	69.63
19%	94.34	106.9	111.7	56.99	72.08	79.26

On the other hand, the evolution of grain shape aspect ratio during the crystal plastic deformation with different loading angles is shown in Figure 24 and Figure 25; and Table 7 gathers the most significant parameters of the fitting.

The rate (mean value) decreases when the plastic deformation degree increases. The smallest aspect ratio is given at the plastic strain of 19% and a loading direction of 0° i.e., the loading along the rolling direction, and the largest aspect ratio is given at 90° the loading direction along the transverse direction. Therefore, the main conclusion that can be drawn is that the grain got elongated along the rolling direction, the direction in which the loading is done. If this elongation is produced when doing the loading on the rolling direction the grain shape value will decrease. However, if the loading angle is done at another angle, the grain will deform diagonally and therefore the grain shape aspect ratio will not suffer such big difference.

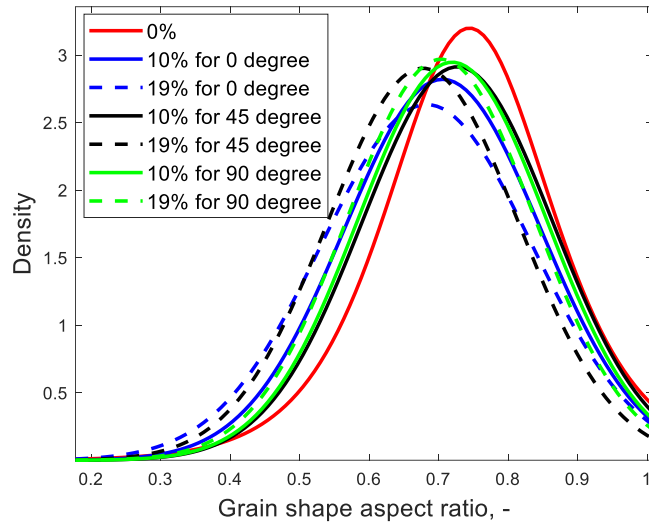


Figure 24: Grain shape aspect ratio evolution with different plastic strains and loading directions.

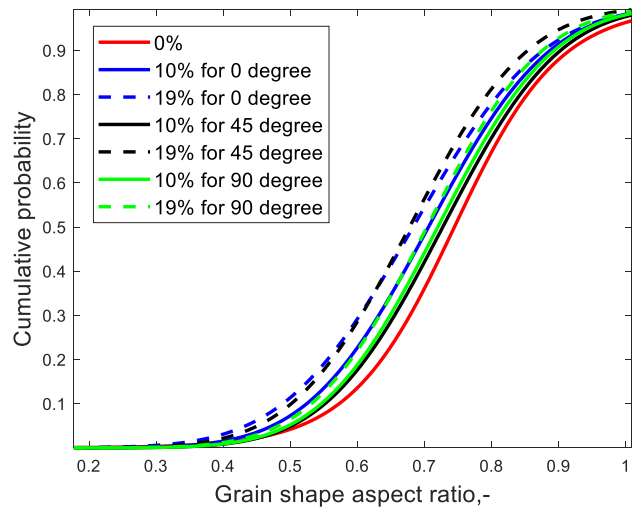


Figure 25: CDF graph of grain shape aspect ratio evolution with different strain degrees and for different loading directions.

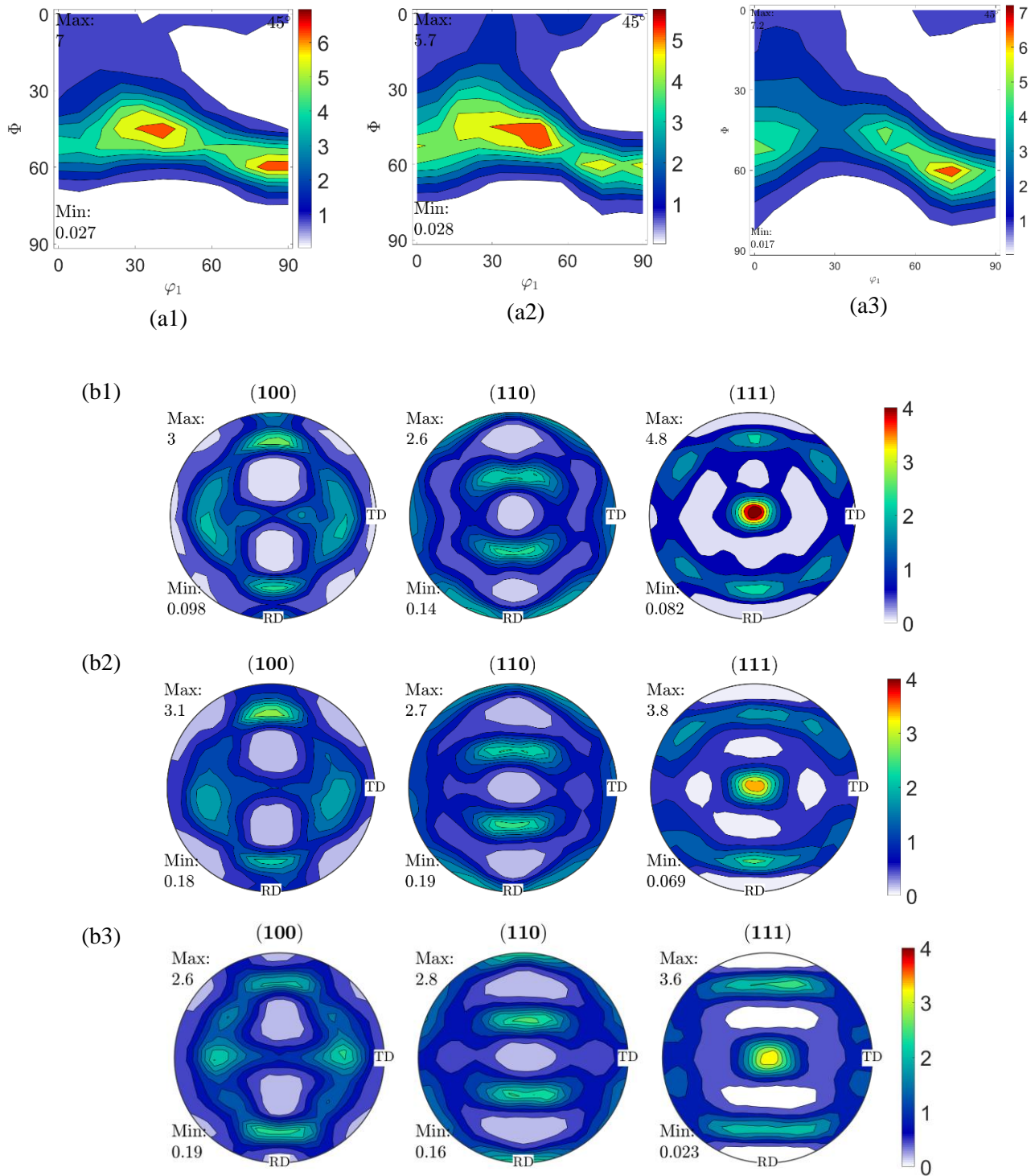
Table 7: Fitting parameters for grains shape aspect ratio at different plastic strain degree for different loading angles.

	Mean value			Standard deviation		
	0°	45°	90°	0°	45°	90°
0%	0.7443				0.5896	
10%	0.7124	0.7046	0.7113	0.6681	0.6861	0.6715
19%	0.6734	0.6825	0.6881	0.6977	0.7147	0.6945

4.3.4. The deformed crystal orientation

Texture evolution results are analysed using MTEX. The ODF figures on phi2=45 section, pole figures for {100}, {110}, {111}, inverse pole figures and the texture index of each loading directions are used. The deformed crystal orientation analysis has been done using the same parameters as for the non-deformed sample texture analysis.

Figure 26, Figure 27 and Figure 28 show the texture evolution in each loading angle and Table 8 shows the main results.



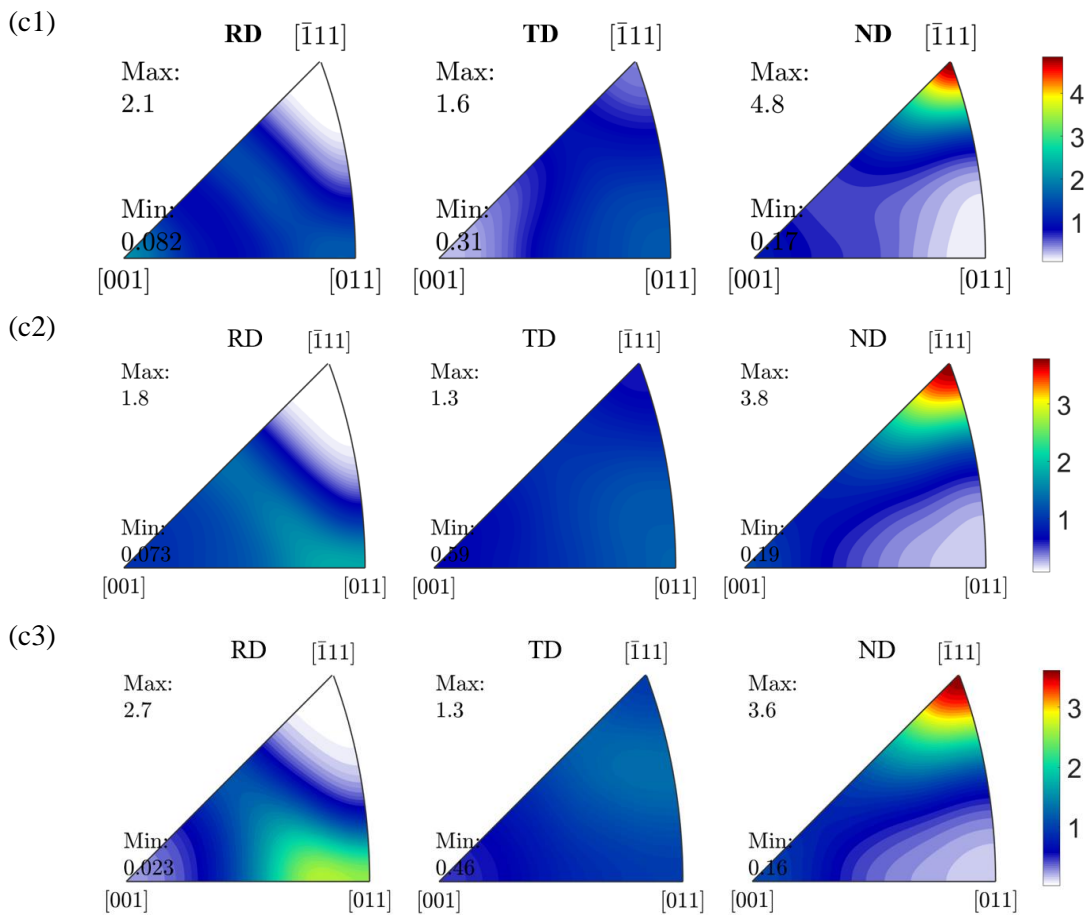
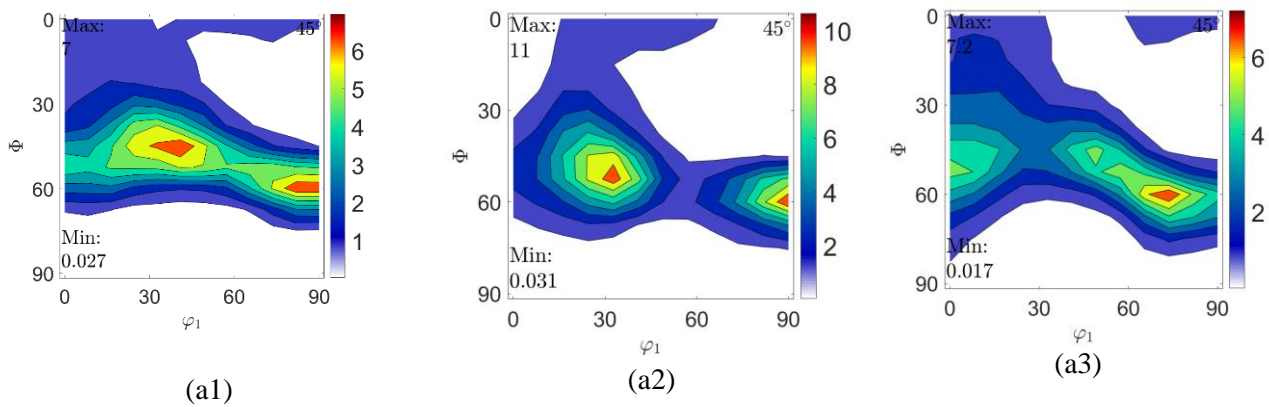
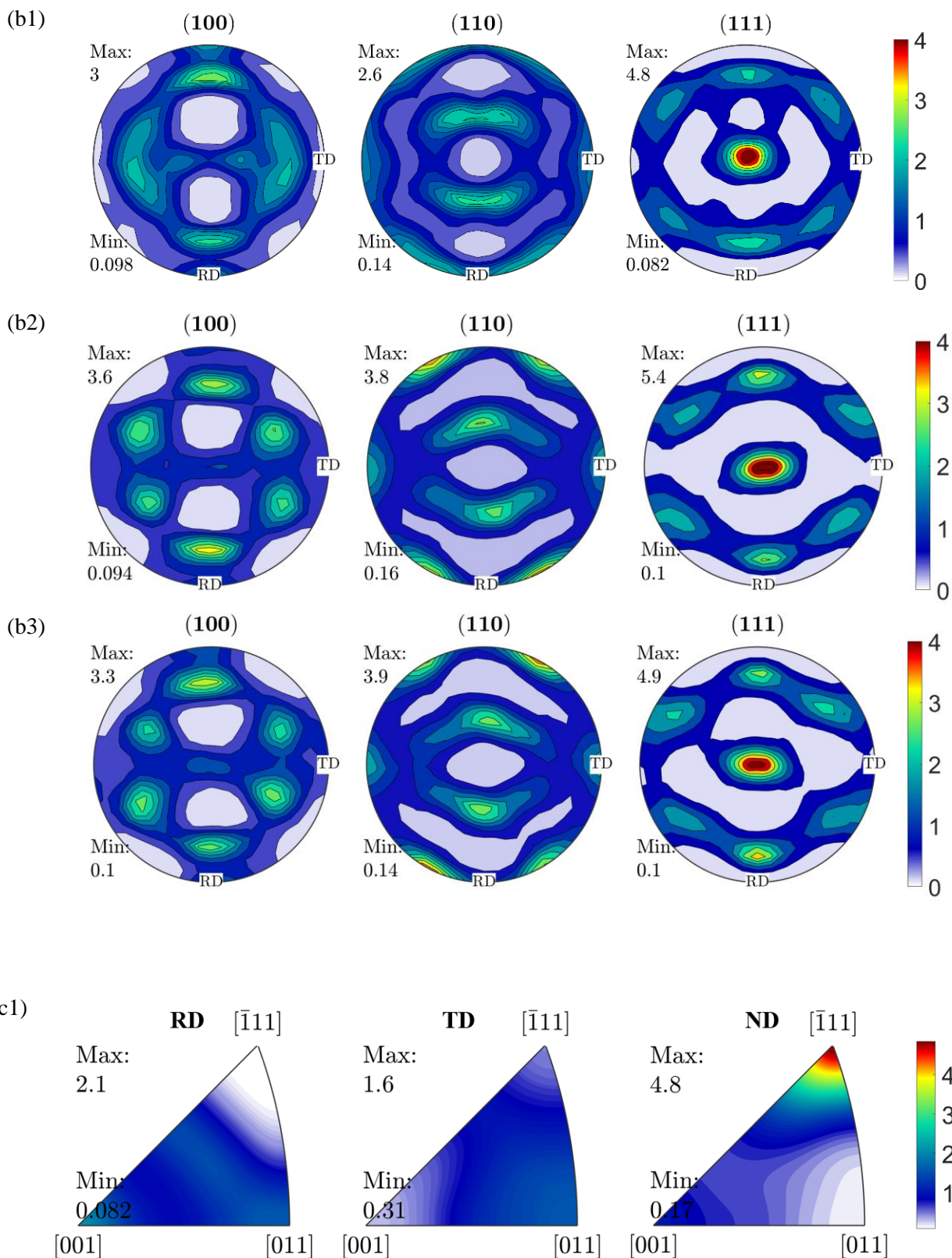


Figure 26: Texture evolution for specimen at loading angle 0° . a:ODF figure at $\phi_2=45^\circ$; b:{100}, {110}, {111} pole figures; c: {110} inverse pole figures; 1: initial state; 2: after 10% deformation; 3: after 19% deformation





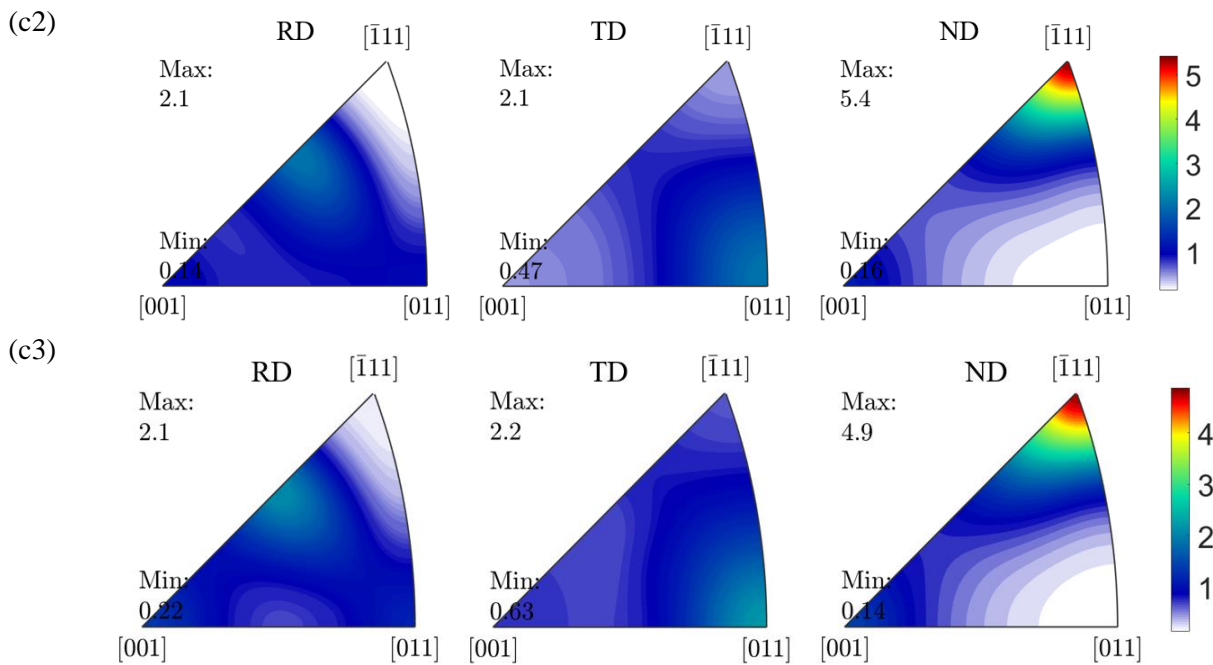
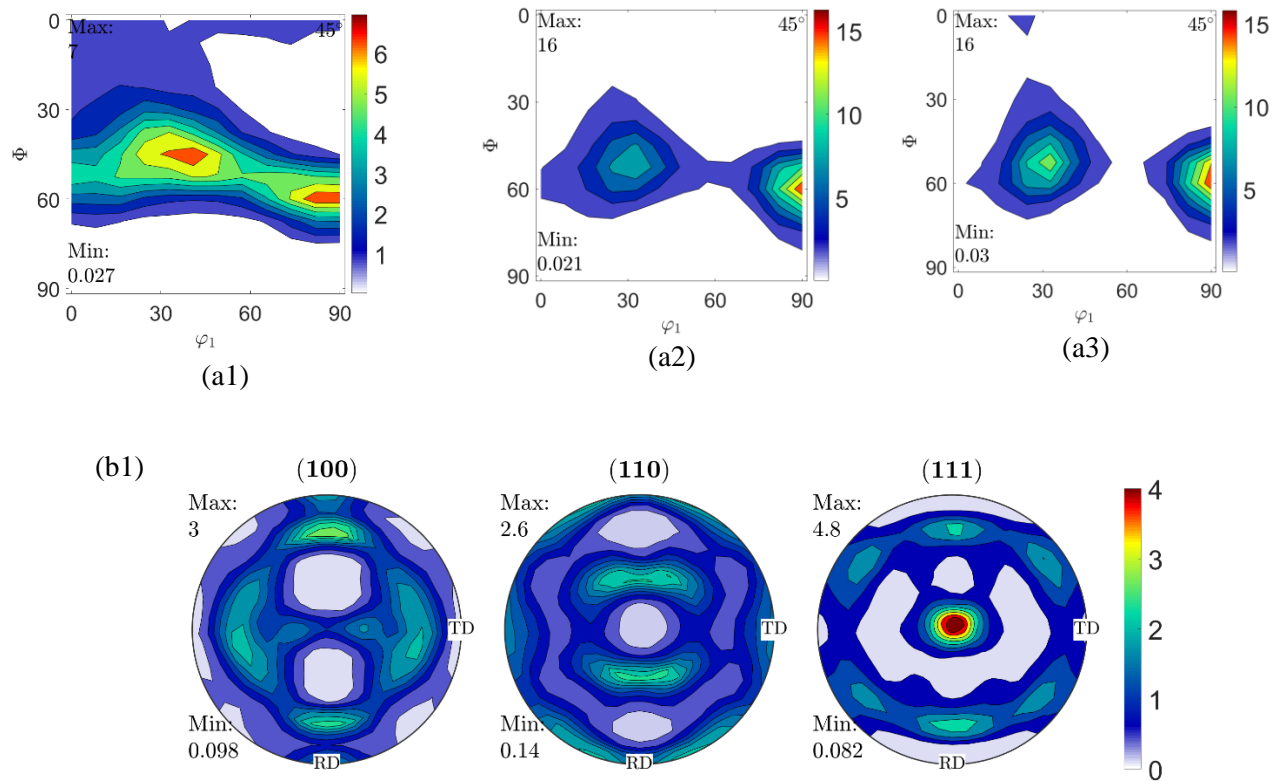


Figure 27: Texture evolution for specimen at loading angle 45° . a:ODF figure at $\phi_2=45^\circ$; b:{100},{110}, {111} pole figures; c: {110} inverse pole figures; 1: initial state; 2: after 10% deformation; 3: after 19% deformation



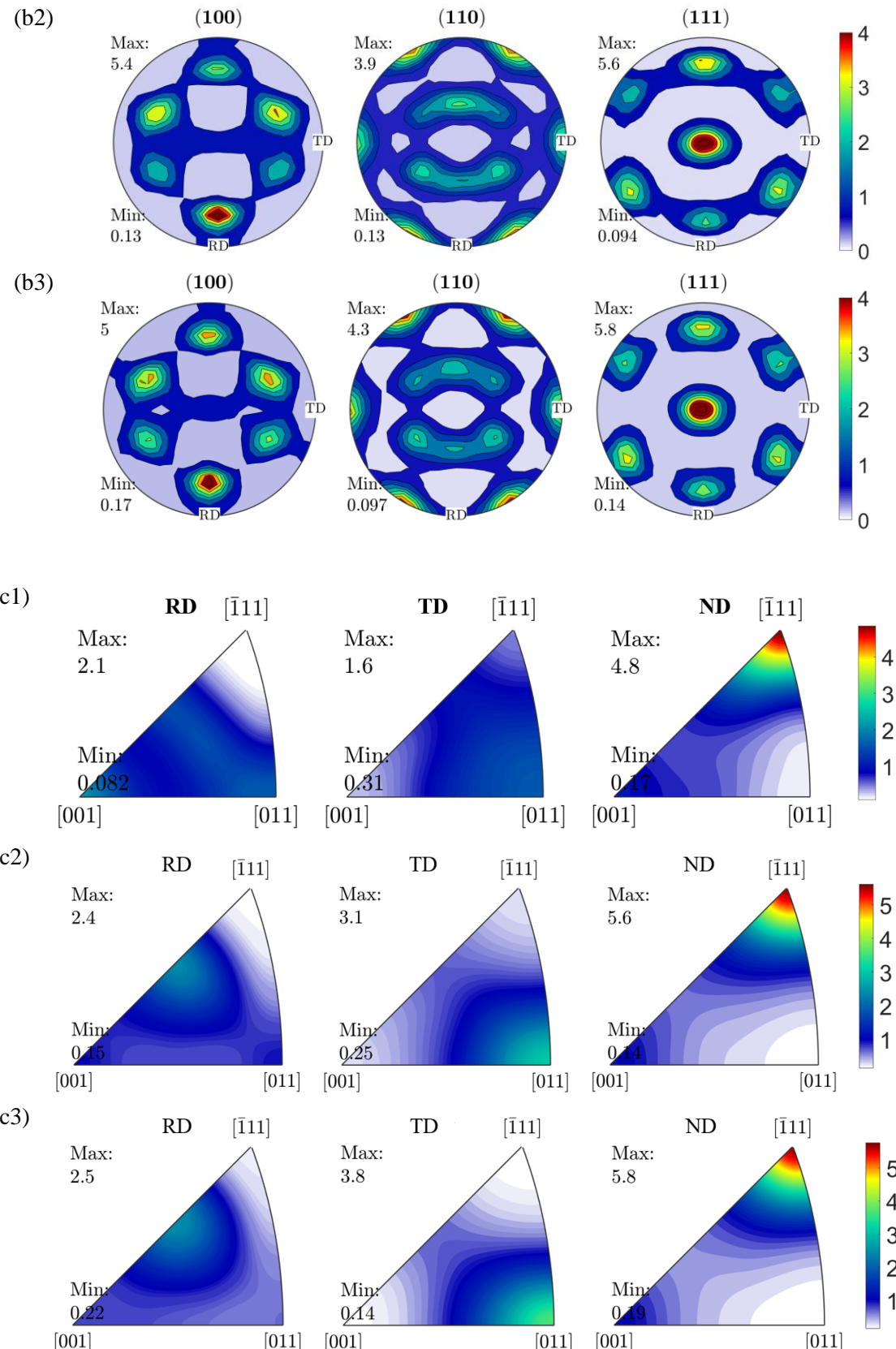


Figure 28: Texture evolution for specimen at loading angle 90°. a:ODF figure at $\phi_2=45^\circ$; b: $\{100\}, \{110\}, \{111\}$ pole figures; c: $\{110\}$ inverse pole figures; 1: initial state; 2: after 10% deformation; 3: after 19% deformation

Table 8: Texture index of orientation distribution function for the measured specimens

	$0^\circ *$	$45^\circ *$	$90^\circ *$
0% **		2.53	
10% ***	2.37	3.05	3.58
19% ***	2.39	2.94	3.77

*) 0° , 45° , 90° are loading angles between the loading direction and the rolling direction.

**) 0% represents for the undeformed specimens.

***) 10%, 19% are plastic strains of the measured specimens.

The main three aspects to analyse grain evolution are texture index, orientation distribution function, the intensity values of all the figures, mainly the ones of the ODF figure and $\phi_2=45$ section, and the position movement of the maximum intensity value spotted in the ODF figures, pole figures and inverse pole figures. The intensity of the texture index defines the density of orientations; thus, it is used to distinguish between strong and weak textures. However, the most important aspect is the position movement which indicates the main orientations, and its movement reveals the texture evolution process.

For the loading angle of 0° the texture index does not vary much. Regarding the density of crystals, the density increases drastically around $<110>/\text{loading direction}$ in the crystal coordinate system as shown in the inverse pole figures, meaning a fibre is generated in the deformation process which is also given in the loading directions of 45° and 90° .

It can be concluded that the loading on the rolling direction generates a rather low texture evolution tendency compared to loading along TD which generates drastic texture evolution.

Following the same tendency as grain shape aspect ratio and grain size, the texture evolution also happens rapidly from 0% to 10% deformation degree, but a slower evolution is given from 10% to 19%.

5. RVE generation with MRAC

5.1. General introduction

To see the effect of grain shape affects the final RVE performance, three different approaches have been used. The three approaches that have been used are equiaxed, preset values and grain shape distribution function. The differences between the input values used in each one of them can be seen in Table 9.

For all three approaches, the used log-normal grain size distribution parameters have been the same. For the first approach, the general/pre-control for grain shape has been the primary equiaxed one, which means the a:b:c values used have been 1:1:1. Secondly, the input values of the preset approach are the mean values of the grain shape aspect ratio obtained by EBSD analysis which are: 1:0.7443:0.7204. Thirdly, the grain shape distribution method uses α and β of the fitted distribution which are 4.7362 and 1.6271 respectively. All of the previous values have been obtained by doing an analysis and microstructure characterisation of the EBSD data of the AISI439 material.

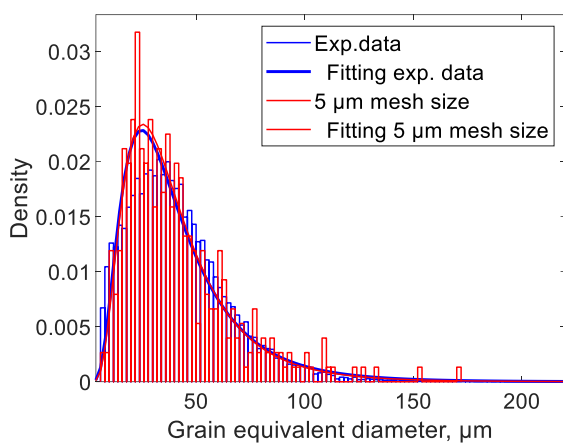
Table 9: Inputs for different shape control

	Mu (μm)	Sigma (μm)	Shape distribution a	Shape distribution b (RD-TD)	Shape distribution c (RD-ND)	Alpha parameter	Beta parameter
Equiaxed	3.56	0.58	1	1	1	-	-
Preset values	3.56	0.58	1	0.74	0.72	-	-
Grain shape distribution	3.56	0.58	-	-	-	4.73	1.62

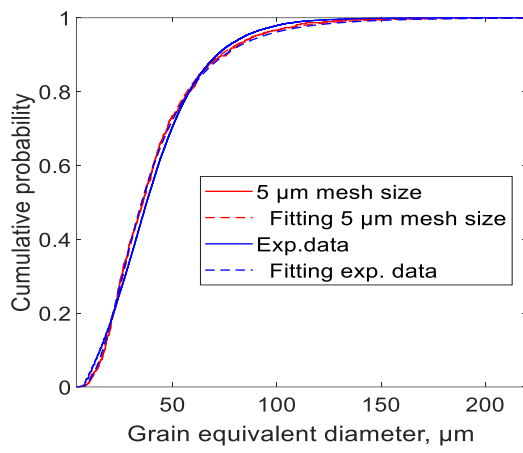
The aim is to find the best distribution and mesh size. To achieve it, mesh sizes of 5 μm , 10 μm , 15 μm and 20 μm have been used to generate RVEs. To reduce the RVE uncertainty, 10 RVEs have been generated with each mesh size for each one of the three grain shape distribution settings. From all the RVEs the best case has been chosen to do further analysis, which is the one with the smallest overall error. To calculate this error, the difference in the input and output values of the main grain parameters has been used, i.e., grain size, aspect ratio, grain shape and texture index.

5.2. Size characterization control

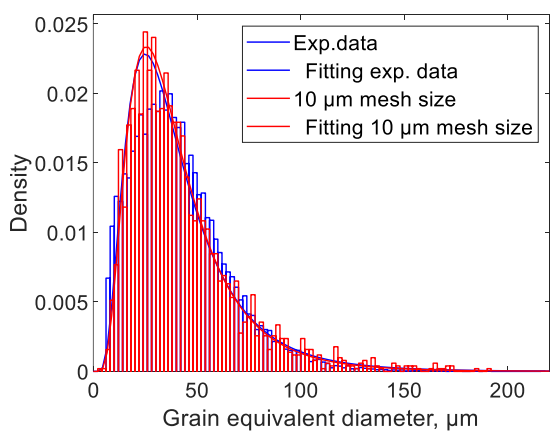
The equivalent diameter is plotted with the third approach to see the difference the mesh size makes. In order to do these plotting the grain shape distribution method has been used (Figure 29). The figures show an overall good fitting of the distribution for all mesh sizes. Moreover, it can be seen that all mesh sizes obtain the nearly the same result as the experimental data. The effects of mesh size on the standard deviation as well as mean value see Table 10.



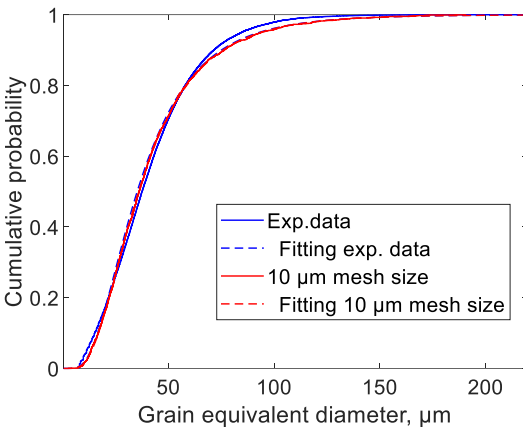
(a1)



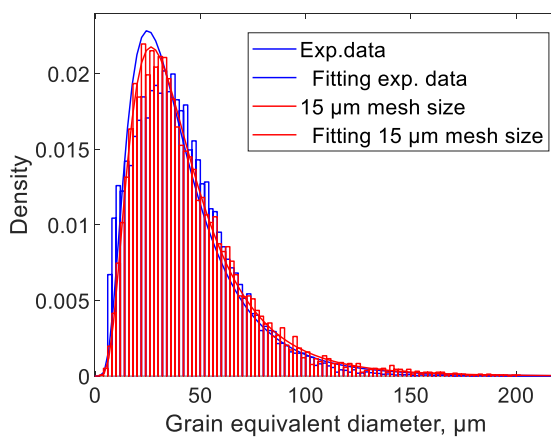
(a2)



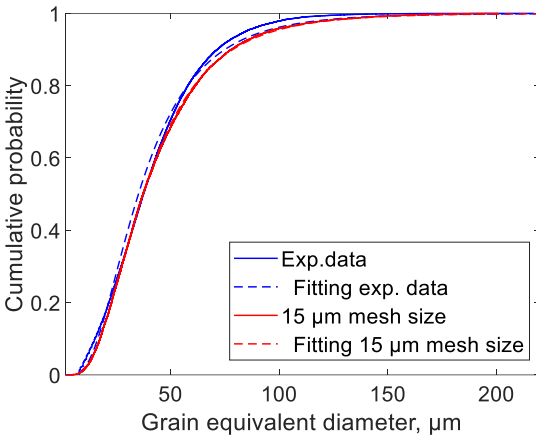
(b1)



(b2)



(c1)



(c2)

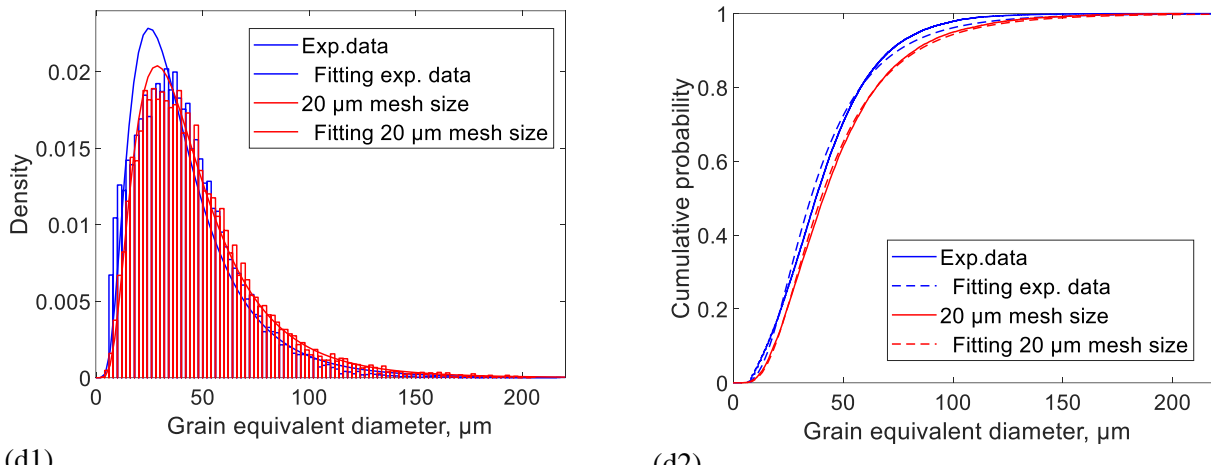


Figure 29: Grain size distribution with of grain shape distribution method compared to exp. data; 5 μm mesh size(a), 10 μm mesh size(b), 15 μm mesh size (c), and 20 μm mesh size (d); CDF (b); 1: bar-chart+PDF, 2:CDF graph

Table 10: Mesh size effect grain size

Mesh size (μm)	Mean value	Standard deviation
5	67.97	32.23
10	67.87	32.41
15	68.11	33.52
20	69.58	34.05
Exp. data	67.46	32.67

5.3. Shape characterization control

In order to see the effect of the mesh size in the grain shape aspect ratio, the results obtained with each size have been compared to the experimental data (Figure 30). As it is observed, all mesh sizes show a very similar distribution, thus, it can be concluded that the mesh size does not play an important role in aspect ratio output.

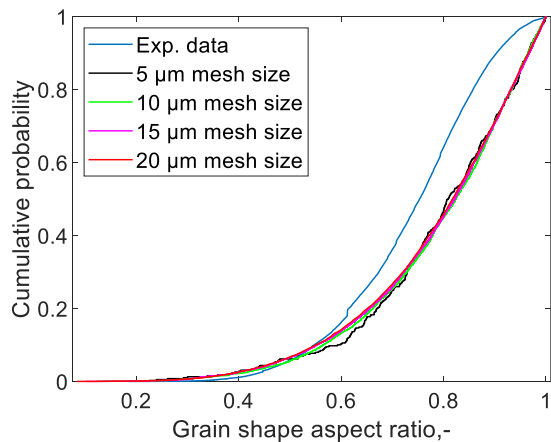


Figure 30: Grain shape with different mesh size

Once the effect of mesh size is analysed, how each control affects the final result is shown in Figure 31

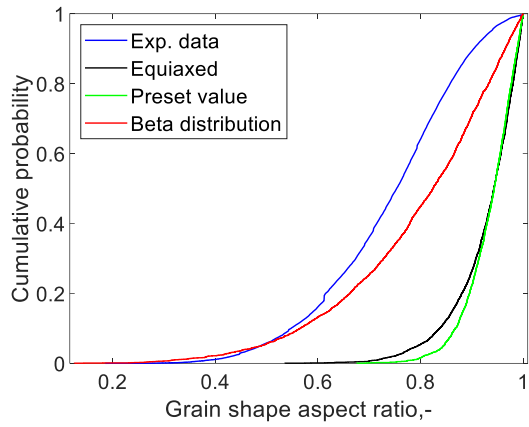


Figure 31: Grain shape effect with 10 μm mesh size and different approaches

Firstly, it can be seen how the effect of mesh size does on the output results. However, as it was expected the different control approaches give very different results. A big difference is seen in the different approaches. The equiaxed and preset values seem to be far off, however the beta distribution gets closer to the experimental value.

5.4. Orientation characterization control

In order to get the control of the orientation, the input values used have been the ones obtained by the experiment.

The difference between the input and output data for texture can be seen in Figure 32, Figure 33 and Figure 34. All the data plotted is the ones obtained with a mesh size of 10 μm . It is shown that the output figures have a higher texture value, meaning a higher concentration of grains with the same orientation. Regarding the overall shape of the pole figures, the experimental one has a rather symmetric look whereas the one of the final RVE does not.

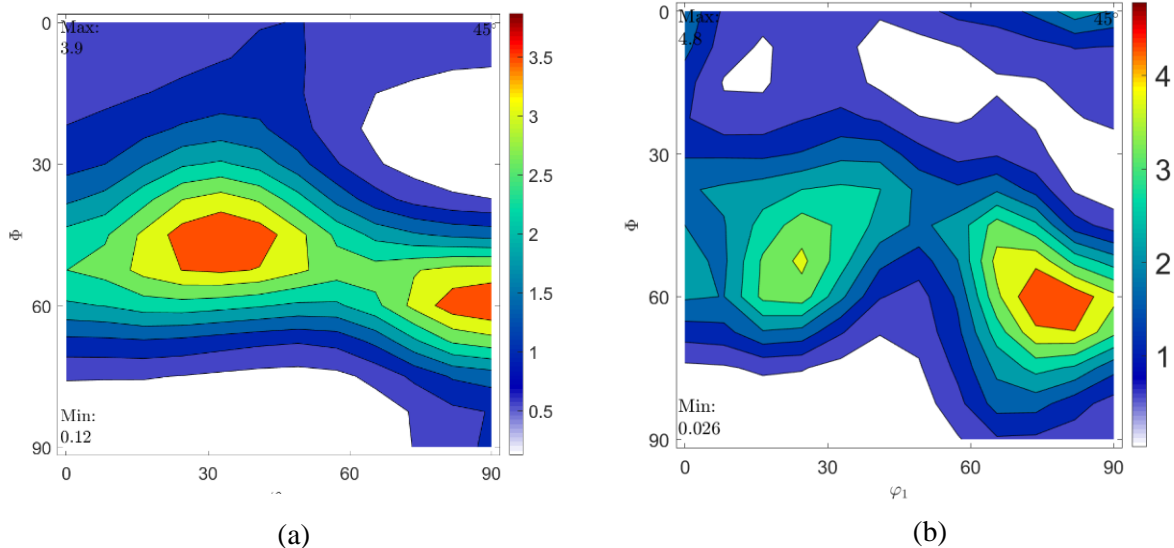


Figure 32: ODF figures with $\phi_2=45$ of experiment data (a) and final RVE (b).

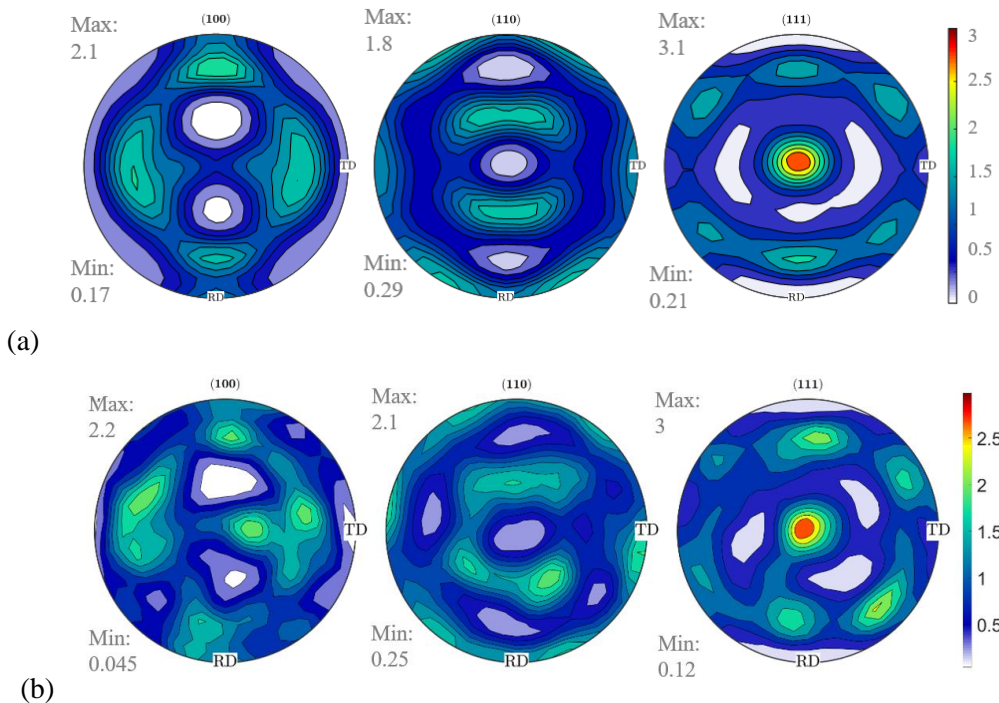


Figure 33: Pole figures of experimental data (a) and final RVE (b)

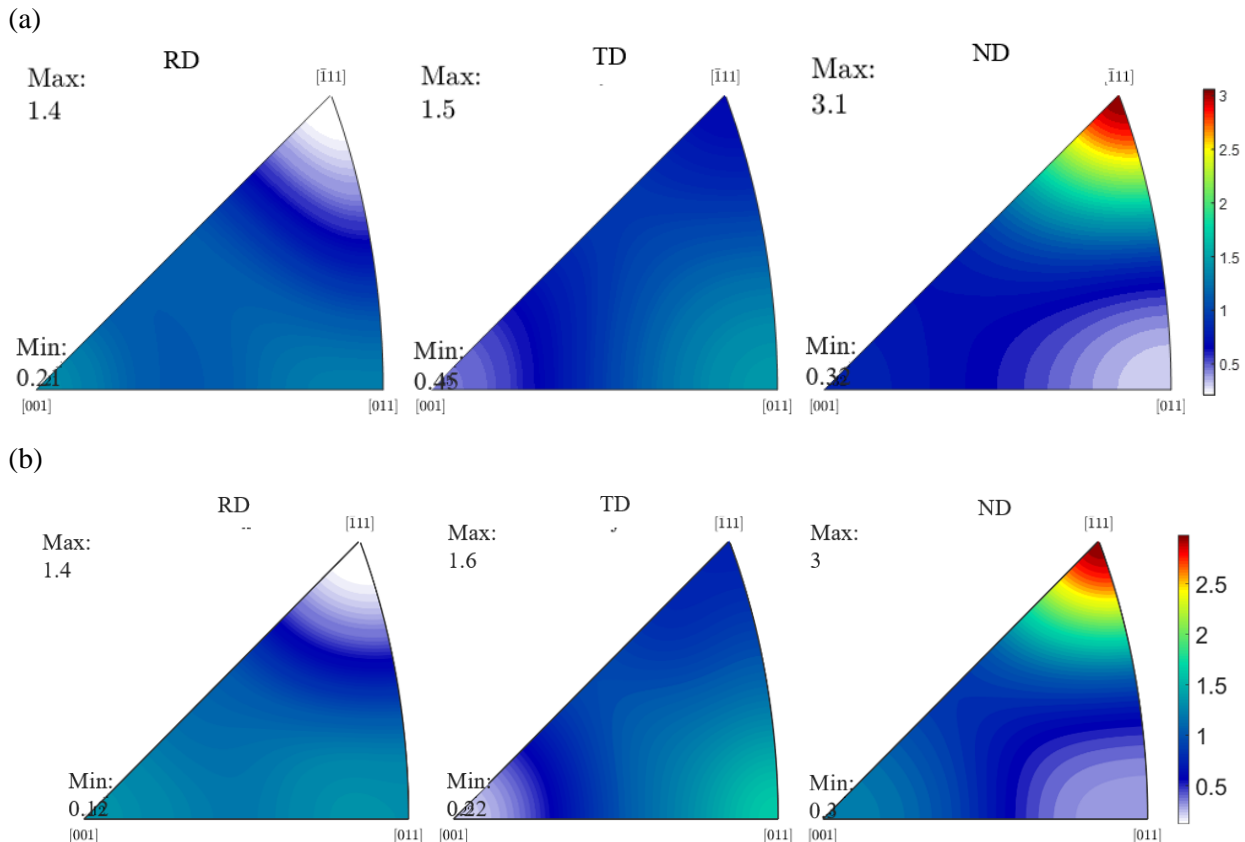


Figure 34: Inverse pole figures of experimental data (a) and final RVE (b)

The specific values of the texture index and the ODF error between the different mesh sizes of beta distribution approach are shown in Table 11.

Table 11: Experiment vs. output beta distribution orientation values for different mesh size.

	Mesh size, μm	Input (Characterized material)	Output (RVE)
Texture index, -	5	2.53	6.4
	10		2.92
	15		1.33
	20		1.16
ODF error	5		1.6
	10		0.92
	15		0.82
	20		0.80

5.5. Evaluation

To evaluate the precision of the final synthetic RVE created by DREAM3D, the output values obtained are compared to the real data.

The relative errors on average grain size (Δ_d), grain shape aspect ratio (Δ_{asp}), ODF error (Δ_{ODF}) and texture index (Δ_t) have been calculated. The individual parameter deviation ΔX is calculated using the equation 17:

$$\Delta X = \frac{|X_{RVE} - X_{ref}|}{X_{ref}} \times 100\% \quad (17)$$

and the best model has been supposed to be the one with the smallest mean error of all variables (Δ) (Equation 18).

$$\Delta = \text{mean}(|\Delta_d|, |\Delta_{asp}|, |\Delta_{ODF}|, |\Delta_t|) \quad (18)$$

To optimize the RVE parameters quantitatively a microstructure representative assessment criterion (MRAC) has been used. This criterion follows two steps: first the RVE uncertainty is minimized and then the RVE generation parameters are optimized. The first step means that even if the input data is always the same the output RVE will change every time. This is why, for the optimization of the optimal input parameters, for each RVE numerical parameter set, 10 RVEs are generated, and the one with the smallest overall error has been used for comparison.

The evaluation of the obtained results is done using the .csv file for grain shape and the .FFT for grain size and orientation obtained through DREAM3D. This .csv contains output values of the grain size, shape and texture; however, it must be taken into account that the results are from a middle stage, thus are not the final results. In order to visualize the quality of these results, they have been plotted using the microstructure representativeness assessment diagram (MRAD) as a radar chart. The outline of the MRAD is assumed to be the reference input information for X_{ref} and assigned to 1[17]. Furthermore, the value X_r (equation 19) of the output RVE feature X_{RVE} on the radar diagram is:

$$X_r = X_{ref}/X_{RVE} \quad (19)$$

Figure 35 shows the effect of each approach on the final result with a mesh size of 10 μm . The main difference between the three approaches is the output accuracy of the grain shape aspect ratio as well as the texture index. Grain size does not change for each approach as it is expected as the input values for grain shape are the same in all three cases. The grain shape aspect ratio seems to be the worst approach with respect to the grain shape aspect ratio. However, both the equiaxed and mean values appear to have a big deviation in the texture index result. The summarized error and grain number are shown in Table 12.

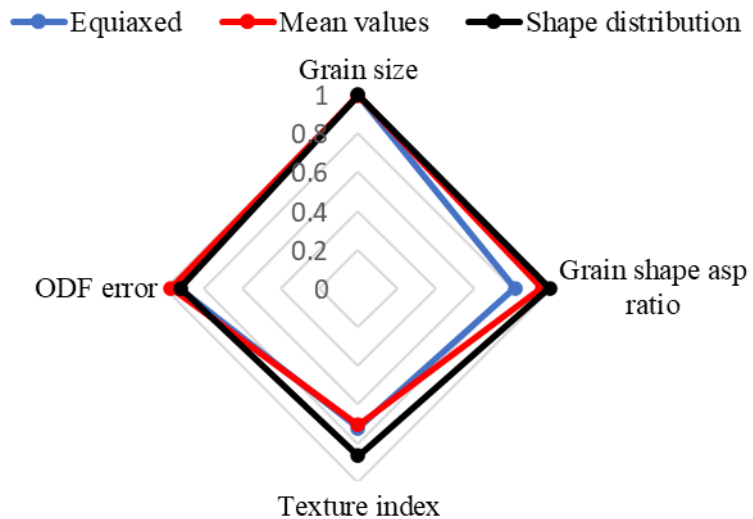


Figure 35: MRAD for output results of different grain shape distribution input methods with 10 μm mesh size.

Table 12: Comparison of output parameters with different approaches with 10 μm mesh size.

		Grain size	Grain shape asp. ratio	ODF error	Texture index	$\Delta, \%$	Grain number
Approach	Equiaxed	0.0005	0.23	0.92	0.27	2.38	2705
	Mean values	0.0026	0.04	0.97	0.29	1.82	2693
	Shape distribution	0.0010	0.0103	0.72	0.15	1.11	2697

As seen in the figure above, the best approach is the shape distribution. Once this is set, the best mesh size must be chosen. The mesh sizes that have been analysed are 5 μm , 10 μm , 15 μm and 20 μm (Figure 36). The summarized errors and grain numbers a matrix is created (Table 13).

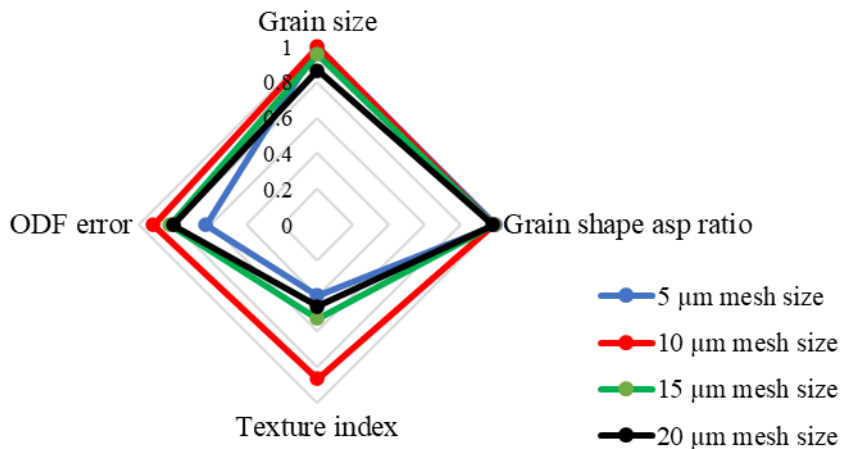


Figure 36: MRAD for mesh size effect on final RVE output results

Table 13: Comparation of microstructural data of intermediate RVE with different mesh sizes.

Mesh size, μm	Grain size	Grain shape asp. ratio	ODF error	Texture index	$\Delta, \%$	Grain number
5	0.01	0.0002	1.60	1.52	4.7	378
10	0.0010	0.0103	0.72	0.15	1.11	2697
15	0.05	0.0119	0.82	0.47	4.12	7832
20	0.15	0.015	0.80	0.53	4.33	15694

As seen in the MRAD figures, mesh size has an important effect on the grain size results. It shows an improvement in the output with small grain sizes. However, it seems to get much better when the mesh size is increased to 10 μm which is concluded to be the best option. For grain shape, the results do not vary depending on the mesh size. However, a big difference is spotted with the texture and ODF error results. Regarding the diagrams, an equilibrium must be found. A very small mesh size obtains bad texture index values, but high values do not make it better either, thus the middle value shows the best results. Overall, the approach with the best output results is the beta distribution method and a mesh size of 10 μm .

6. Development of MRAC

As mentioned in the chapter above, the .csv document used to do the analysis only offers a rough estimation of the final results. Therefore, for the final output results of the RVE, Los Alamos FFT file has been used. This file also allows to analyse the grain shape orientation. The following chapters explain how the process is done and the obtained results.

6.1. Introduction of post-process

Once the RVE has been generated, the analysis of the results has to be made using MTEX. RVEs are the representation of the microstructure in 3D. Therefore, to do a comparison with the initial experimental EBSD data the adaptation to 2D must be done (Figure 37).

This process has been done with MATLAB. The main process is to slice the final RVE in 64 different layers and to analyse each one of them independently, obtaining the most characteristic grain parameters, i.e., grain size, grain shape and orientation. In each layer, the grains are represented as cubes and following the initial microstructure analysis, very small cubes (grains) have been disregarded as well as the grains located at the edges. Figure 38 shows how the fitting of the ellipses is done and how the cube grains look like as well as which cubes should be disregarded for being too small. The data of all the layers are then combined to achieve a data set that has an overall outlook of the whole RVE. These final output values are representative and accurate to the generated RVE.

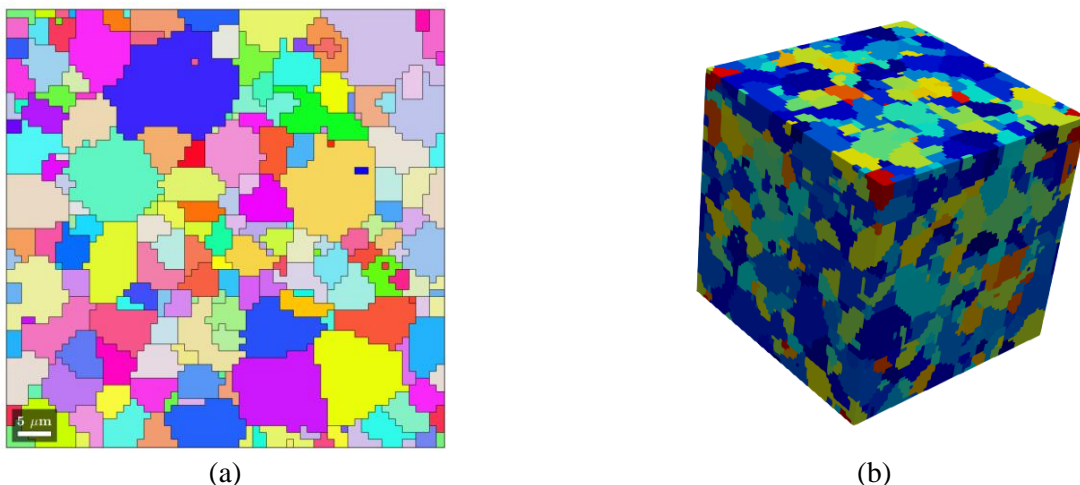


Figure 37: Grain map of RVE, 2D (a) and 3D (b).

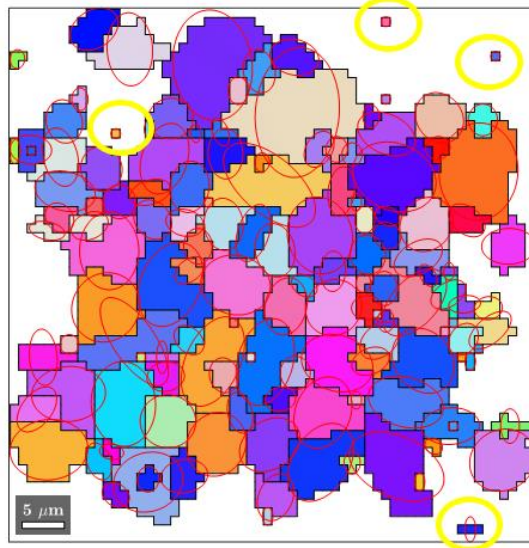


Figure 38: 2D RVE fitting on ellipses disregarding edge grains. Pixels marked with yellow are disregarded.

6.2. Grain shape aspect ratio

With the analysis of the final RVE data, the results obtained on the grain shape aspect ratio are considered very accurate as seen in Figure 39. The figure shows that both input and output values follow the same distribution with a peak point at around 0.6 at the final RVE. The final RVE seems to have more grains gathered around the mean value and a smaller overall scatter, so the grains will have a more uniform shape.

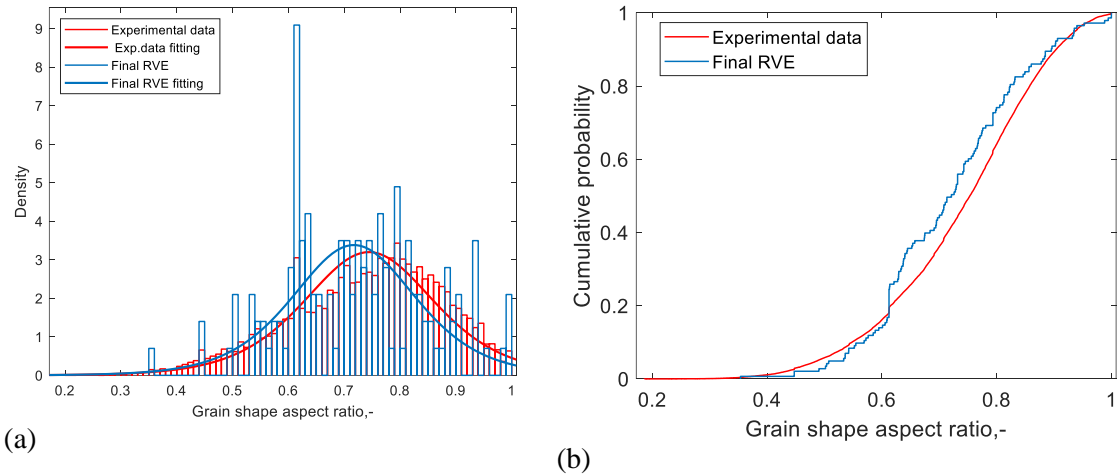


Figure 39: Experimental vs. final RVE grain shape aspect ratio results, bar chart+PDF (a) and CDP (b).

6.3. Grain tilt angle control

Grains are fitted as ellipses for grain shape. These ellipses have different orientations depending on the microstructure. Grain shape axis orientation or tilt angle refers to the orientation between the longest axis of the fitted ellipse and the reference direction, i.e., RD (See Figure 40). This variable gives the information of how the grains are orientated along the RVE in order to see the effect on the final performance.

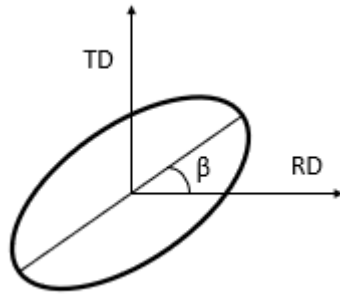


Figure 40: Grain axis orientation

For input, the experimental tilt angle data has been divided into groups of 15 degrees. Once the data is divided, a weight value is given to each group. The value of this weight depends on the density of the tilt angle, i.e., a higher density requires a higher input weight. In the case of the grains having a very strong orientation, this weight must increase highly, and the sigma value must be small. For a not so strong shape orientation, this weight should be smaller, and a higher sigma should be used [18].

The grains have first to be fitted in ellipses. The quality must be ensured in this step as it will be of great importance for the tilt angle analysis. This new variable has been analysed using the Los Alamos FFT file and the following results are obtained (See Figure 41).

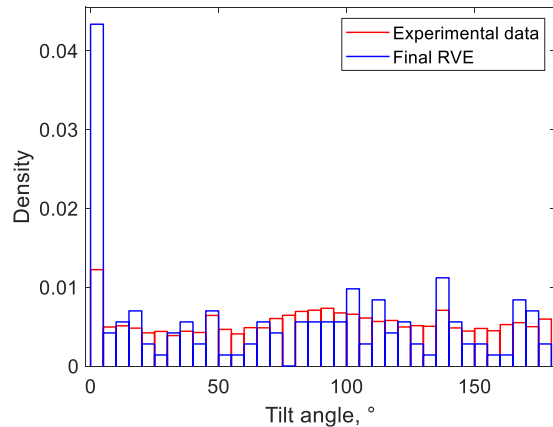


Figure 41: Tilt angle input vs output values

As it can be seen, the shape orientations of the grains throughout the RVE are quite uniform in all directions. Firstly, the peak point for the grain tilt angle in 0° can be seen as the biggest difference between the two distributions, which means the control of this specific angle is not achieved completely. The overall tendency of the output angle results is similar to the experimental ones. However, the final RVE tends to have a lower number fraction in most cases.

6.4. Evaluation of distribution features

With the aim of getting a better evaluation of the output results in regard to the input values, the MRAC graphs have been further developed taking into account the Kolmogorov-Smirnov test. This evaluation method, for each potential value, compares the proportion of values less than x with the expected number predicted by the standard normal distribution [19]. The parameters that define the KS test are H, p, KSSTAT and CV.

- H: Comparison between the data in vector x with a standard normal distribution.
- p: Null hypothesis significance testing.
- KSSTAT: Kolmogorov-Smirnov statistic. The maximum difference between the curves.

- CV: Cut-off value to determine if KSSTAT is significant.

KS testing method does a hypothesis seen in equation 20 and 21.

$$H_0: P = P_0 \quad (20)$$

$$H_1: P \neq P_0 \quad (21)$$

Where P is the unknown distribution, and P_0 is the particular distribution. H_0 means that the data follows the specified distribution and H_1 that the data does not follow the specified distribution.

If $\text{KSSTAT} > \text{CV}$, the hypothesis H_0 is rejected. However, when $\text{KSSTAT} < \text{CV}$ the hypothesis H_0 is accepted.

The analysis of the data has been done using MATLAB. Table 14 shows the results obtained by the KS test when doing a comparison of the different approaches and mesh sizes with the experimental data. KS-test seems to be accurate to calculate the maximum error between two distributions, however a quantitative value of the overall distribution is not given, thus, the k value is the only one that will be used for further analysis.

Table 14: Grain shape aspect ratio results for KS test.

Grain shape aspect ratio				
	Mesh size	h	p	k
Equiaxed	5	1	7.04×10^{-141}	0.68
	10	1	0	0.66
	15	1	0	0.69
	20	1	0	0.68
Pre-set values	5	1	1.05×10^{-151}	0.69
	10	1	0	0.73
	15	1	0	0.69
	20	1	0	0.72
Beta distribution	5	1	1.5×10^{-14}	0.20
	10	1	11.46×10^{-105}	0.22
	15	1	5.4×10^{-2491}	0.21
	20	1	0	0.20

The equiaxed and pre-set values have a high deviation number comparing to the beta distribution. This means that the maximum space between the experimental data distribution and the final RVE output data distribution is three times less in the case of the latter. The first two approaches have very similar error numbers; however, the pre-set method seems to be a bit higher. The similarity of these two approaches can be because the input grain is already quite equiaxed.

With the new evaluation method, the test is done using the data from Table 15 and the values of grain size, grain shape aspect ratio, and grain shape orientation.

Table 15: Grain size and shape data of final RVE obtained by KS testing.

	k
Grain size	0.09
Grain shape aspect ratio	0.12
Grain shape orientation	0.16

The results show a low gap between the experimental and final RVE values. The lowest value is given between the input and output values of the grain size. Then the grain shape aspect ratio would come with a higher value and finally, the grain shape orientation has the biggest error. The main conclusion is that all three parameters have a great outcome, but still have a small margin where improvement can be made. However, these results are promising and mean a very good overall control of all the parameters has been achieved.

The representation of the final RVE is the following (See Figure 42). The numerical setting and the optimal RVE parameters are listed in Table 16.

Table 16: Numerical settings and microstructure features of the optimal RVE of AISI439.

Mesh size, μm	RVE size, μm^3	Grain number				ODF error
		Grain size, μm		Grain shape aspect ratio		
μ	σ	α	β			
Input	3.56	0.58	4.73	1.62	2.5362	0.5573
RVE	3.05	0.43	5.53	0.62	3.2283	

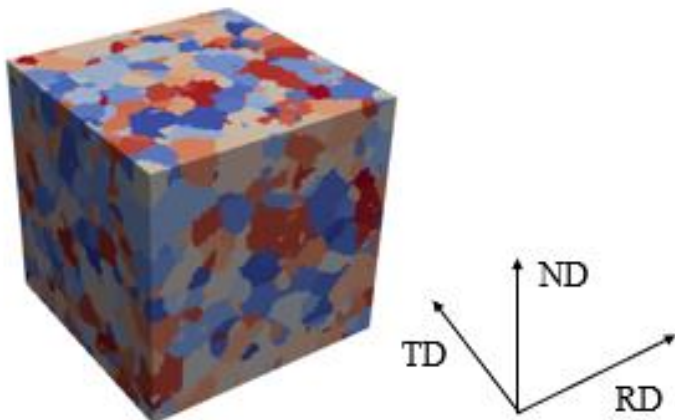


Figure 42: Grain map of optimal RVE with the improved evaluation method

7. CP model predictions

Once the final RVE and its error are calculated, its final performance has to be analysed, for which some crystal plasticity simulations have been run. In order to run the CP simulations, the parameters that have been used have been taken from the literature[20]. The values are the following (Table 17):

Table 17: Crystal plasticity parameters of AISI 439 calibration by polycrystal simulation with CPFFT at RT

Parameter	1/m	$\dot{\gamma}_0(s^{-1})$	$\tau_0(\text{MPa})$	α	$\tau_s(\text{MPa})$	$h_0(\text{MPa})$
Value	77.26	2.78×10^{-4}	105	1.2	234	800

Firstly, in order to see how the performance of the literature RVE model, a CP simulation is run to see its true stress-true strain curves and see the difference between the two (Figure 43). As it can be seen, the results obtained when running the same simulation with the same data are different. The results that are obtained show lower values during the whole stress-strain curve. However, in both cases the highest value is achieved with a loading angle of 45° followed up by 90° and finishing up by the 0° loading angle i.e., rolling direction.

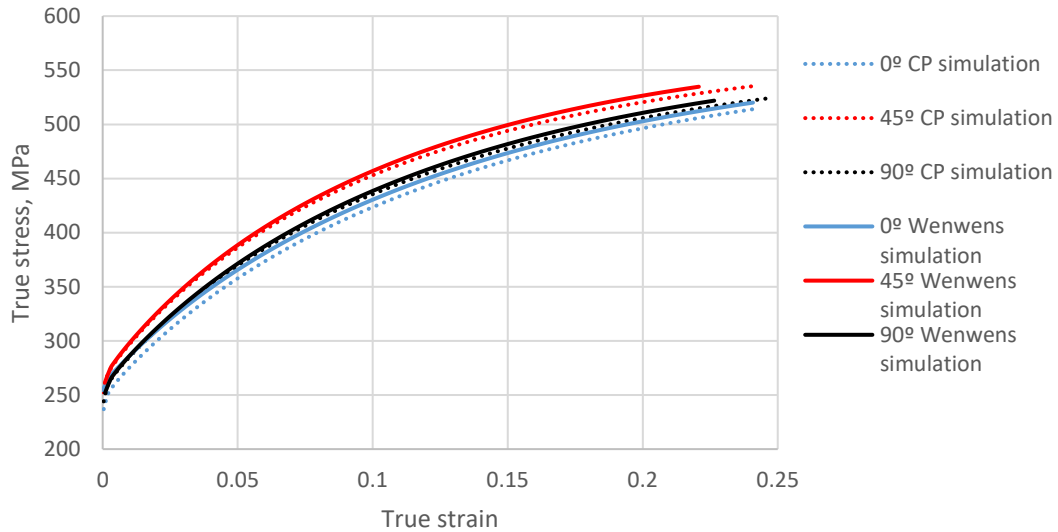
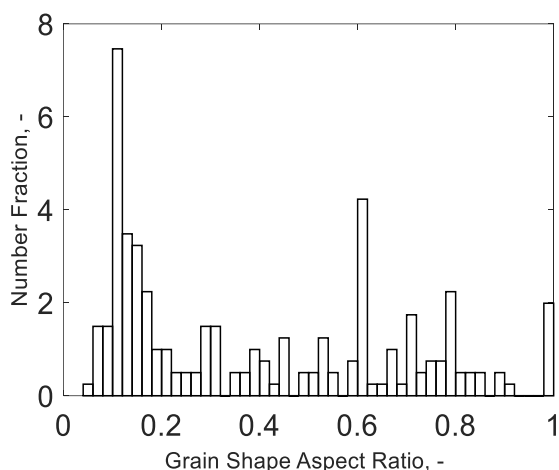


Figure 43: True stress-strain curve for CP simulation vs. other RVE configuration at different loading angles

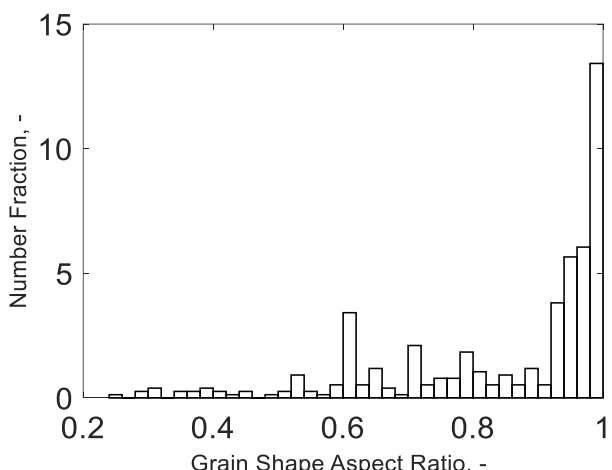
8. Microstructure parametric study

8.1. RVE with variant grain shape control

In order to see the control of grain shape in other cases, two extreme cases have been considered: the grain shape aspect ratio is assumed as 1:0.1:0.1 for the drastically elongated grains along RD and 1:0.9:0.9 for grains that are nearly equiaxed. To minimize any variables, both cases are assigned with the same microstructural features set to the reference material except the grain shape aspect ratio variant. The approach that has been followed has also been the beta distribution method to make the results comparable. As it can be seen in Figure 44 as the input value for grain shape aspect ratio changes so does also the output. It can be seen that in both cases the peak is now given at 0.1 and 0.9 respectively, therefore it can be concluded that the control over this variable is achieved even in extreme cases. To see the RVE obtained in each case see Figure 45.



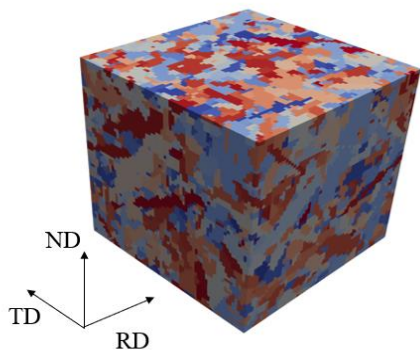
(a)



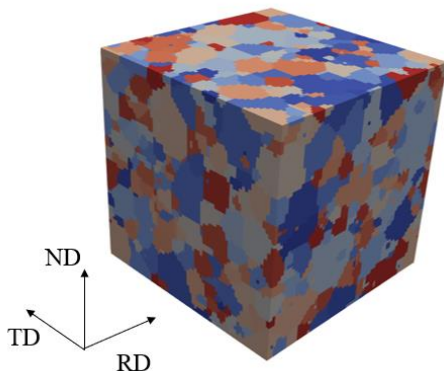
(b)

Figure 44: Grains shape aspect ratio output data with input of 0.1(a), and 0.9 (b).

From the figures above it can be seen that the control with the grain shape aspect ratio of 0.1 is not accurate as nearly no values are at the range of 0.1. Therefore, the control for very elongated grains has not been fully achieved. However, when doing it with an input value of 0.9 it can be seen how most of the grains get closer to the set values and most of them are from the range of 0.7 to 0.9. This means that this control has worked however its effect is not 100% accurate. Regarding the two graphs a peak for the values of 0.6 can be seen. This peak is given in all cases and seems to be an output error of the actual DREAM3D program.



(a)



(b)

Figure 45: RVE generated with aspect ratio of, 0.1 (a) and 0.9 (b)

8.2. RVE with variant grain axis orientation control

The grain axis orientation is another parameter that should be controlled. To see the actual real control other three cases have been analysed. In this case, an input grain tilt angle of 45° , 90° and 180° have been used and have been compared to the no control graph. To see the real effect very elongated grains have been used with the shape aspect ratio of 1:0.1:0.1.

Figure 46 shows the difference in the output in each case. As it can be observed, when inserting an input of 45° the output values tend to have a big increase in that area. Moreover, the angles located further away from this value get a drastic decrease. In the case of 90° , the same pattern can be seen. On the other side, an increase in the tilt angle of 0° can also be spotted in all cases. This happens because of an internal error of DREAM3D.

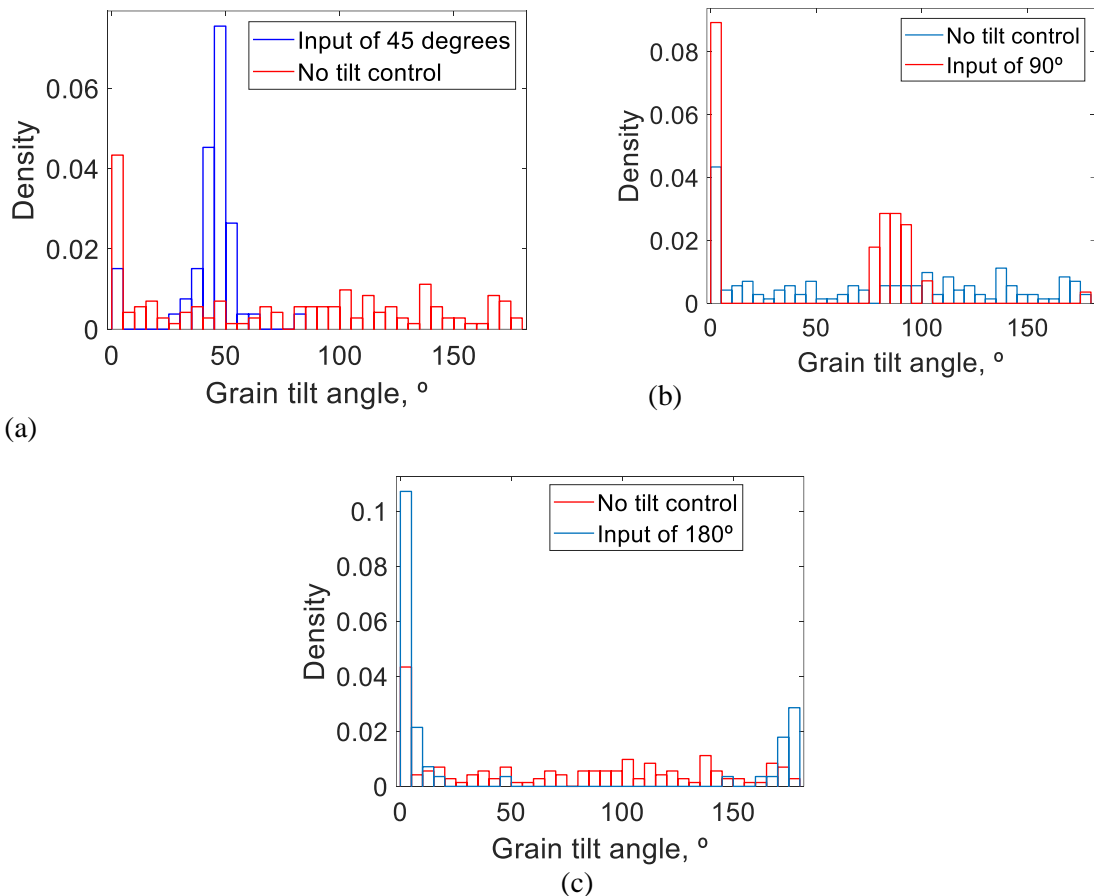


Figure 46: No tilt angle control vs. 45° input (a); 90° input; and 180° input

And the RVEs obtained are shown in Figure 47. From the figures the overall tendency of the figures can be seen clearly, therefore it is concluded that the axis orientation control has been fully achieved.

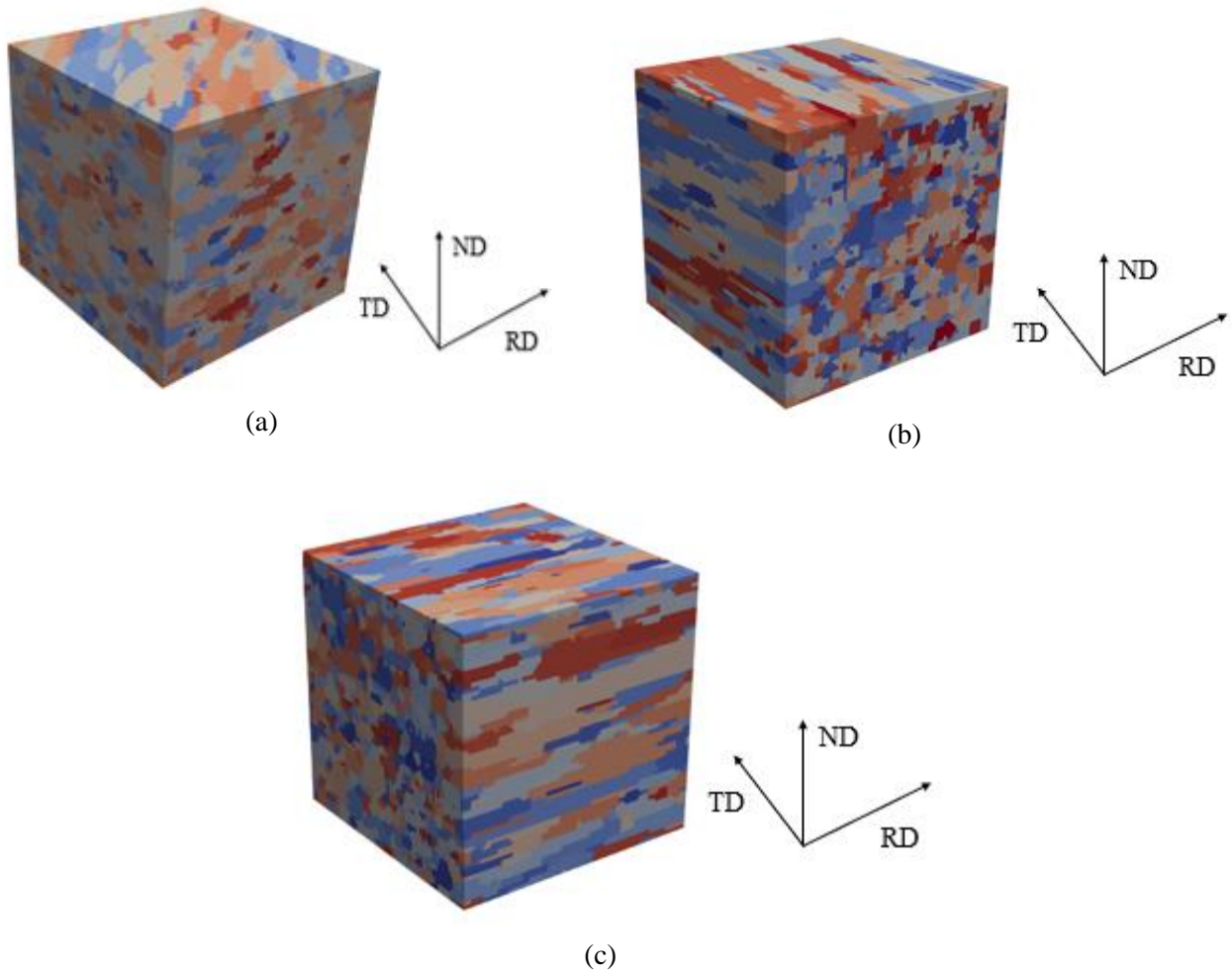


Figure 47: RVEs for grain tilt 45° (a), 90° (b) and 180° (c).

9. Economic report

This section details the economic report of this thesis, which ultimately has some practical relevance as it shows the cost that is needed in order to generate an accurate RVE and can be compared to other methods that are used to select and analyse the behaviour of materials. It must be cleared that no experiments had to be done for the analysis of this project as experimental results have been obtained from literature and only the analysis of it had to be done. All the accountable costs of the project are gathered in Table 18.

Table 18: Cost of the project resources.

OFFICE MATERIAL	
Desktop computer with Windows 10 Pro x 7 months	151 €
MATLAB R2020a- academic use license	35 €
Microsoft Office 365 license	50 €
TOTAL COST OF THE PROJECT	236 €

10. Conclusions

In this study, the different approaches to control grain shape and its effect on the final predictions have been studied, taking into account the grain size and texture parameters simultaneously. The main conclusions that can be drawn regarding the set objectives are the following:

- Very good control of the output grain shape aspect ratio has been achieved. After analysing different mesh sizes, it has been concluded that it does not affect the final output result. However, regarding the three different approaches, the beta distribution function has shown to be three times better than the other approaches. Moreover, this method has been validated for other extreme cases, where grains are extremely elongated or equiaxed and the results show a good control too.
- Good control of the grain size has been achieved using methods from literature. In addition, the effect of mesh size has been analysed. It has been seen how a smaller mesh size gets better output results with enough element numbers. On the other hand, regarding the different distribution approaches, they do not show any difference in the results. Therefore, the standard analysis method should also obtain good results for the beta distribution method.
- Grain shape orientation control has been analysed and achieved. The analysis shows generally good control. However, some further research must be done to avoid amounts of trials to obtain the control parameters, i.e., tilt angles and weights.
- Different methods to evaluate parameters have been used. Firstly, the MRAC method from literature has been used, then it has been further developed to KS test. This last evaluation method in comparison to the first one takes into account the whole distribution when calculating the error. However, from the four parameters given by this method, only one has been quantitative enough to do a comparison.
- Finally, a program to accurately analyse the final grain parameters in the generated RVE has been made. This program cuts the 3D RVE into 2D sections, then fits the 2D grains into ellipses. The analysis of each layer of the RVE are combined to get a distribution of the final result that gives an overview of the final RVE microstructural parameters.

11. Future lines

Regarding the conclusions that have been stated in the previous chapter, some future lines can be set for further analysis in the control of an RVE.

Firstly, further analysis has to be done to achieve a better grain axis orientation in DREAM3D. The process and the parameters needed for the control and their effect on the result have been analysed. However further analysis should be done in order for DREAM3D to obtain more accurate output results.

On the other hand, to get a great RVE involving all the different variables, the control of the correlated and uncorrelated misorientations have to be analysed as they have not been considered in this project and are also a variable that affects the plastic behavior.

The final texture evolution and anisotropy behaviour simulations of all the different RVEs should be done to see the final effect that each parameter has on the final prediction results and to see if the crystal plasticity simulation parameters from literature are suitable for this new model.

Finally, once the steps above are achieved it would be useful to follow up by controlling an RVE with precipitates and seeing if the control of it can be done in the same way or how the input parameters have to be modified in these cases to achieve a realistic synthetic microstructure.

12. Personal evaluation of the traineeship

The bachelor's degree traineeship program carried out between Mondragon Unibertsitatea and Aalto University has given me the opportunity to develop my autonomous learning capacities as well as to develop my skills to work in a team. My skills and knowledge in materials science and programs such as MATLAB and DREAM3D have increased immensely.

To start with I've learned how to characterize and model a material starting from its microstructural features. Furthermore, in order to generate an accurate RVE, many different controlling methods have been carried out which has taught me how to do an evaluation of results regarding different evaluation criteria. Moreover, regarding software that I've started using from scratch, I've been able to learn how to use and control the various features of DREAM3D from scratch as well as to get a light overview of how to use DAMASK to do the post-processing analyses of materials; besides, I've also improved my MATLAB skills obtained through the previous years. This has increased my autonomous learning ability.

I would also like to mention the support of both my host and home university and the phenomenal guidance of professors Juhne Lian and Joseba during all stages of the thesis; and I would like to do a remark on the insight help of Wenqi regarding everyday work and for all of the support, patience and knowledge transmitted.

To conclude, doing this internship has served me to apply my knowledge acquired during my Bachelor and to get a small glance at the investigation sector in the labour world. It's been a well-rounded experience.

13. References

- [1] A. Butz, S. Lossau, B. Springub, and F. Roters, "On the Modeling of Dual Phase Steels: Microstructure-based Simulation from the Hot Rolled Sheet to the Deep Drawn Component," *Int. J. Mater. Form.*, vol. 3, no. 1, pp. 73–76, 2010, doi: 10.1007/s12289-010-0710-7.
- [2] J. Lian *et al.*, "Plasticity and failure behavior modeling of high-strength steels under various strain rates and temperatures: Microstructure to components," *Procedia Struct. Integr.*, vol. 13, pp. 1421–1426, 2018, doi: 10.1016/j.prostr.2018.12.295.
- [3] S. F. Mason, *Crystal structure determinations*, vol. 282, no. 5736. 1979.
- [4] W. Liu, "Modelling of the evolution of texture and microstructure features during plastic deformation of bcc steels by crystal plasticity models," *Rheinisch-Westfälische Technische Hochschule Aachen Institut für Eisenhüttenkunde*, 2016.
- [5] T. K. L. Delannay, M.A. Melchior, J.W. Signorelli, J.-F. Remacle, "Influence of grain shape on the planar anisotropy of rolled steel sheets – evaluation of three models," in *Computational Materials Science*, 2009, pp. 739–743.
- [6] E. R. Davies, *Introduction to texture analysis*. 2008.
- [7] H. J. Bunge, "Mathematical methods," in *Texture analysis in Material Science*, 1982.
- [8] S. I. Wright, "Orientation Texture," *Encyclopedia of Condensed Matter Physics*. 2005, [Online]. Available: <https://www.sciencedirect.com/topics/engineering/pole-figure>.
- [9] E. of Encyclopaedia Britannica, "Anisotropy," *Britannica*. [Online]. Available: <https://www.britannica.com/science/anisotropy>.
- [10] "Tensile testing of metallic materials. Method of test at ambient temperature," in *European standard EN 10002-1*, Brussels, 2001.
- [11] X. Gastañares, "Automotive AA5753 alloy plasticity analysis based on the RVE technique i," Aalto university and Mondragon university, 2020.
- [12] J. Lian *et al.*, "An evolving non-associated Hill48 plasticity model accounting for anisotropic hardening and r-value evolution and its application to forming limit prediction," *Int. J. Solids Struct.*, vol. 151, pp. 20–44, 2018, doi: 10.1016/j.ijsolstr.2017.04.007.
- [13] F. Roters, P. Eisenlohr, T. R. Bieler, and D. Raabe, *Crystal Plasticity Finite Element Methods: In Materials Science and Engineering*. 2010.
- [14] S. Steel *et al.*, "thyssenkrupp Materials (UK) Ltd Processing / Welding," *International Journal of Corrosion*, vol. 447, no. 4. pp. 1–3, 2017.
- [15] H. H. J. Huh, Y.J. Kim, "Measurement of R-values at Intermediate Strain Rates using a Digital Speckle Extensometry.," in *Dynamic Behavior of Materials*, 1st ed., 2011, pp. 317–322.
- [16] E. J. Savoie, J. J. Jonas, "Evolution of R-value during the tensile deformation of aluminum," in *Textures and Microstructures*, 23rd ed., 1995, pp. 149–171.
- [17] W. Liu, J. Lian, N. Aravas, and S. Münstermann, "A strategy for synthetic microstructure generation and crystal plasticity parameter calibration of fine-grain-structured dual-phase steel," *Int. J. Plast.*, vol. 126, no. October 2019, p. 102614, 2020, doi: 10.1016/j.ijplas.2019.10.002.
- [18] S. A. H. Motaman and C. Haase, "The microstructural effects on the mechanical response of polycrystals: A comparative experimental-numerical study on conventionally and additively

- manufactured metallic materials," *Int. J. Plast.*, vol. 140, no. October 2020, p. 102941, 2021, doi: 10.1016/j.ijplas.2021.102941.
- [19] M. help Documents, "Kolmogorov-Smirnov test." <http://matrix.etseq.urv.es/manuals/matlab/toolbox/stats/kstest.html>.
- [20] W. Zhang, "A Multiscale Modeling Study on the Effects of Temperatures and Strain Rates on Plastic Behaviors of Steels," 2019.

Appendix A: Scope statement

This scope defines the technical, administrative, and legal conditions for the project to materialize under the specified conditions, avoiding possible different interpretations from those desired. This corresponds to the Final Project of Mechanical engineering Degree carried out at Aalto University, whose title is “3D synthetic microstructure generation involving grain size, shape, and orientation representation”.

A.1 Scope of the thesis

The project that is to be carried out consists of the RVE generation of AISI439 steel. The analysis should focus on two main areas which are the grain size control and grain shape control.

By this approach a better understanding of how to generate accurate RVEs should be determined in order to generate more accurate mechanical properties in the future in comparation with the current approaches that are being used.

It will also include a thorough analysis of the advantages and drawbacks of the control used and will set the improvement lines for the grain shape control as well as texture index control.

This project is classified as a research project.

A.2 Project conditions

A.2.1 Project management

To encourage an efficient and controlled project management several points have been agreed and will be fulfilled:

- The project will be planned with a Gantt chart and this planning will be available for the tutor and supervisor.
- A clear workflow will be generated at the start of the project in order to get a clear idea of the working path.
- There will be a regular weekly update meeting with the supervisor of about 2 hours to discuss updates and current progress, and another scientific discussion will be done in a group with PhD students and a senior researcher of around 2 hours. Furthermore, once a month a meeting will be done to explain the current progress with the senior researcher. Finally, a presentation will be held every month in front of other PhD students to share opinions and updates on current work.

A.2.2 Safety measures and regulation

First of all, the trainee must complete a labour safety prevention course. The industrial installations in which the all the experimental process will be carried out (either manufacturing, assembly or testing) will have to fulfil the regulations listed in the following lines. These regulations define the safety rules that must be fulfilled, the necessary personal protective equipment and the prevention measures.

- Law 31/1995, of labour risk prevention.
- Law 54/2003, of the reform of the legal framework on labour risks.
- Royal ordinance 485/97, which establishes the minimum safety and health requirements of the workplace.

On the other hand, when any manufacturing or testing machine will be used, it is necessary to comply with the safety manual that contains the rules regarding its operation. It should be noted that all of these machines must contain the CE marking, which is governed by royal ordinance 1644/2008, which establishes the rules for the marketing and commissioning of the machines. Finally, the technical characteristics table of each machine must remain visible.

A.3 Resources and material specification

For the development of this project a variety of elements must be available which are listed below:

- Desktop computer with Windows 10 Pro
- MATLAB R2020a – academic use license
- Microsoft Office 365 license
- Dream3D
- Paraview 5.9.1
- Damask 2.0.2
- 2 sheets of 1x2 m of AISI439
- Zwick/Roell INSTRON 3369 tensile test machine
- GOM Aramis DIC
- Mechanical grinders and polishers
- EBSD microscope

The cost of each one of the used materials is listed in section 9 of the report.